PREPRINT UCRL-81152 Rev. 1

Lawrence Livermore Laboratory

THE SIGNATURES OF THE VARIOUS REGIONS OF THE OUTER MAGNETOSPHERE IN THE PITCH ANGLE DISTRIBUTIONS OF ENERGETIC PARTICLES

Harry I. West, Jr.

December 11, 1978

This is an invited review paper prepared for presentation at the American Geophysical Union Chapman Conference, "Quantitative Modeling of Magnetospheric Processes," 19-22 September 1978 at La Jolla, California.

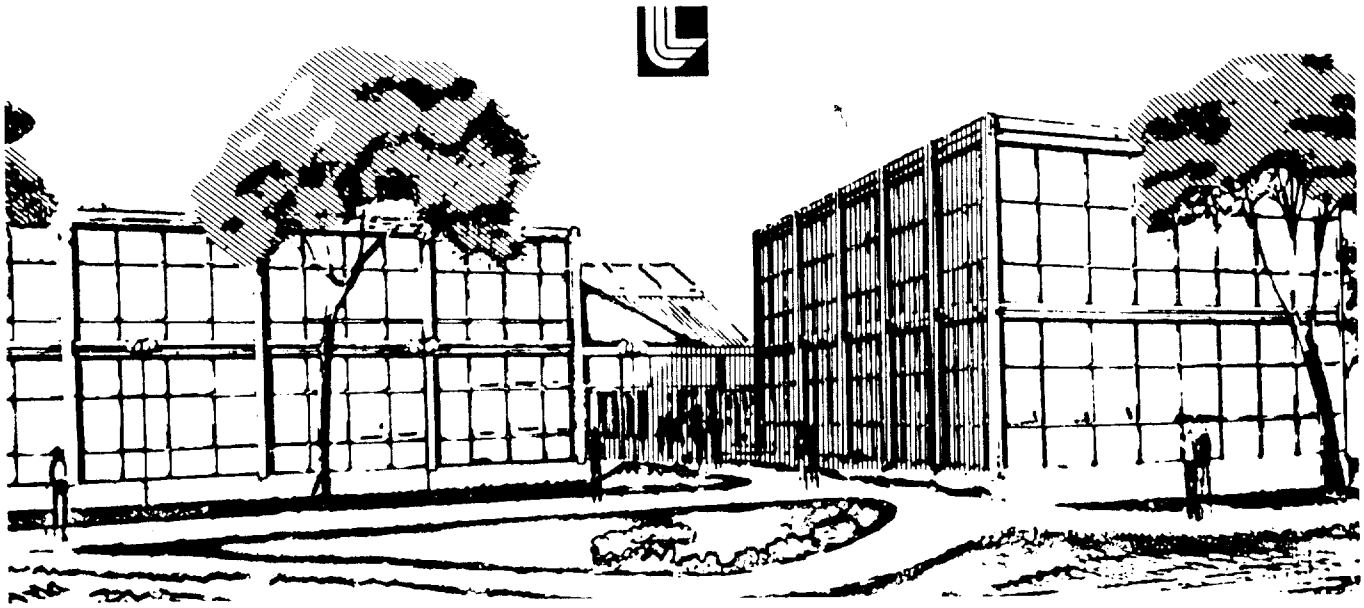

THE SIGNATURES OF THE VARIOUS REGIONS OF THE OUTER MAGNETOSPHERE IN THE PITCH ANGLE DISTRIBUTIONS OF ENERGETIC PARTICLES

Harry I. West, Jr.

Lawrence Livermore Laboratory, University of California
Livermore, California 94550

Abstract. An account is given of the observations of the pitch angle distributions of energetic particles in the near equatorial regions of the earth's magnetosphere. The emphasis is on relating the observed distributions to the field configuration responsible for the observed effects. The observed effects relate to drift-shell splitting, to the breakdown of adiabatic guiding center motion in regions of sharp field curvature relative to partial gyro radii, to wave-particle interactions, and to moving field configurations.

Introduction

The signature that the magnetosphere leaves in the pitch angle distributions (PAD's) of azimuthally-drifting energetic particles can be used as an important diagnostic tool in the understanding of the magnetic field configuration. This paper examines these signatures primarily emphasizing the PAD's of energetic electrons rather than protons. The reason for this is straightforward. For example, the rigidity $B\rho$ for 79-keV electrons, the lowest energy electrons that will usually be considered, is 0.154 γR_E. In contrast, the $B\rho$ for the lowest energy protons that will be considered, 100-150 keV, is 8 γR_E. The electrons are the more useful of the two for probing the fine structure of the magnetosphere since in the outer regions of the magnetosphere the protons are more subject to breakdown of the adiabatic invariants than are the electrons. Of course, in principle, one could use low-energy proton data but then the results are strongly affected by convection.

The effects presented fall mainly into three categories. The first has to do with shell splitting and how the electrons at various pitch angles drift through the distorted magnetosphere; in this case the particle motion is completely adiabatic. The second case pertains to the breakdown of adiabatic motion in those distant regions in which the gyroradius of the particle is no longer small relative to the field-line curvature. The third case pertains to scattering through wave-particle interactions, especially those periods of time when the particles are close to the magnetopause; this case is more difficult to treat theoretically and is less strongly emphasized in this review.

This review relies heavily upon Ogo-5 observations by the Lawrence Livermore Laboratory (LLL) experiment during 1968 and 1969 covering the equatorial regions out to 24 R_E [West et al., 1973a; West and Buck, 1974]. The experiment consisted of a 7-channel magnetically-selected electron spectrometer and proton telescope located on a scanning boom. The success of the Ogo-5 data analysis has depended greatly upon the ready availability of good magnetometer data from the UCLA experimenters covering all periods of data acquisition. When appropriate, work other than our Ogo-5 results are cited. Most of the results presented are from data acquired close to the geomagnetic equator. This leaves out

the whole problem of what happens to the field and particle distributions at the edge of the polar cap near the earth and the ingenious methods that people have applied in the study of the associated field topology. For example, there is the use of the so called "trapping boundary" which has been widely used to define, ostensibly, the change from closed to open field lines. Also, during solar electron events the observation of transition from a double to a single loss cone as the satellite entered the polar caps has been used extensively to define the transition to open field lines; we will not have much further to say about these methods.

In the first part of this paper we present the studies of PAD's of energetic electrons in the equatorial regions of the magnetosphere from the magnetopause on the dayside of the earth to about 17 R_E on the nightside of the earth. We first discuss how drift-shell splitting alters the PAD's of drifting electrons. We then follow the eastward azimuthal drift of the electrons, starting on the morning side of the earth, examining their encounter with the magnetopause in terms of drift-shell splitting, emphasizing the high-latitude regions near noon, and noting the resultant evolution of the PAD's in the extended afternoon magnetosphere. In the premidnight magnetosphere we examine PAD's during quiet times showing the marked effects of drift-shell splitting.

Near midnight we show spatially-dependent quiettime PAD data which have been analyzed in terms of field modeling and particle trajectories. Next we discuss the PAD changes observed during substorms and show how these changes are used to infer the field configurations during the various phases of the substorm. This first part of the paper ends with a discussion of the PAD effects observed post-midnight.

In the second part of the paper we present a potpourri of proton and electron observations, with the emphasis on the signatures that moving boundaries leave in the distributions of energetic particles. We first present a brief picture of our knowledge of the PAD's of energetic protons throughout the magnetosphere. We then discuss the observation of the spatial gradients of energetic protons by means of the east-west effect and how their temporal variations can be interpreted in terms of moving boundaries. This is followed by the use of energetic-particle directional distributions in the magnetotail to infer the motion of field-line structures through the use of the Compton-Getting effect.

Pitch Angle Distributions of Energetic Electrons

PAD Survey

We begin with a brief survey of the LLL Ogo-5 electron observations at all local times to provide a framework for what follows. Figure 1 shows the Ogo-5 PAD survey. A few words on nomenclature are in order. We have termed the bell-shaped distribution a normal loss-cone distribution because in the early history of space physics it was the distribution normally expected, since the measurements at that time were mostly in the near-earth regions; also the distribution is shaped much like a normal frequency distribution (when presented in a Cartesian plot $0\text{-}180^{\circ}$) and is peaked normal to the field direction thus emphasizing the term normal distribution. Occasionally in the literature this

has been called a pancake distribution. The distribution depleted near 90^{o} pitch angles we call a butterfly loss-cone distribution, reflecting its shape ($j(\phi)$ vs ϕ, $0\text{-}360^{o}$) in a polar plot. It has been called an anti-loss-cone distribution which is a misnomer since the loss cone is usually empty. The butterfly distribution has also been called cigar-shaped which seems particularly inappropriate. Finally, we have the isotropic distribution, a universally-accepted term. However, in the context of the work presented here, the term isotropic does not necessarily mean that the loss cone is filled with precipitating particles.

Let us now discuss Figure 1. We start with the morning sector and proceed eastward following the azimuthal drift of the electrons. In the morning sector we find the normal PAD out to the magnetopause. In the early afternoon we find the butterfly PAD at extended distances and by dusk we find the butterfly PAD extending inwards to 5.5 to 7.5 R_E depending upon energy. The dashes at the more extended distances refer to the crossover from butterfly to normal for ~79-keV electrons, and the inner band of dashes refers to the crossover for ~822-keV electrons. Note that this band extends across the entire nighttime sector. You will also notice that in the extended early evening sector the butterfly PAD prevails whereas in the corresponding region past midnight we frequently find isotropy. Obviously the data show the marked effects of drift-shell splitting, and in the more distant nighttime magnetosphere we have the effects of substorms. We expand on this later. Some aspects of this survey were known prior to the Ogo-5 observation; for example, Serlimitsos [1966] and Haskell [1969] had observed the butterfly PAD in the nighttime magnetosphere. However, the observations in the afternoon magnetosphere are unique to our Ogo-5 experiment, and it took Ogo-5 observations [West et al., 1973a; West and Buck, 1974] to put together the picture for the total magnetosphere. We want to keep the survey in mind as we proceed with the rest of the presentation.

Drift-Shell Splitting — Basic Ideas

The idea of drift-shell splitting was probably put forward initially by Northrop and Teller [1960] but has received major impetus through the efforts of Roederer [e.g. 1967]. (Also see Schultz [1972] for later references.) The particle motion under discussion is completely adiabatic. One examines the drift shells of the particles of various equatorial pitch angles and finds that if he breaks the azimuthal symmetry, exemplified by the near-earth dipole field, that the degeneracy of the drift paths is removed.

The picture of separation of drift shells is usually explained by examining the drift paths of 90^{o} particles along with particles of small equatorial pitch angle. In the first case the equatorially-mirroring particles must drift at constant B as shown, e.g., by the data of Fairfield [1968] in Figure 2, thus moving from 9 R_E near noon to ~6.5 R_E near midnight. For the second case we find that in evaluating the integral for the second invariant ($I = \oint \sqrt{1-B/B_m}\, ds$) that I is close to being equal to twice the bounce path of the particle, that is twice the distance along the field line between mirror points. Of course, these particles must conserve the first invariant, also, and thus drift at constant B at their mirror point. Roederer [1967] has calculated

these effects using the Mead [1964] model. The results are shown in Figure 3. Here e.g. we see 37° equatorial pitch-angle particles ($\cos \alpha_e = 0.8$) moving from 8.1 R_E to an equatorial crossing of 9.2 R_E at midnight at an equatorial pitch angle $\lesssim 20^\circ$ ($\cos \alpha_e \approx 0.95$), and 78° particles ($\cos \alpha_e = 0.2$) initially, moving to 7.1 R_E at 68°.

Lets proceed to see how the PAD's transform from the dayside to the nightside of the earth. We first examing PAD's on the dayside, then transform these data to midnight, and finally compare them with measurements. Figure 4 shows a radial profile of the $j_\perp$ (differential flux perpendicular to $\vec{B}$) fluxes on an inbound pass of Ogo 5 on March 30, 1968. First note the abrupt increase in particle flux at the magnetopause ~11 R_E. In the outer trapping regions the data are characterized by the negative radial gradients that we have come to associate with diffusion. In Figure 5 we see the corresponding PAD's. The very pronounced energy dependence evident for the lowest two L shells (3.06 and 3.32) and to a lesser extent L = 3.89, we now know is due to the special way that whistler-mode radiation interacts with electrons in the plasma sphere as shown by the theoretical results of Lyons, Thorne, and Kennel [1972] and experimental results of, e.g., Lyons and Williams [1975]. In the more extended magnetosphere (L = 8.38 and 9.18) a narrowing of the PAD's with increasing energy is evident. We have not attempted to determine the cause of the effect but expect that it is related to diffusion.

To make the transformation of the electron PAD data to midnight we use the calculated results of Roederer [1967] in Figure 6, making use of Liouville's theorem. We choose the shell crossing the equator at 7.4 R_E at midnight as the place to generate the PAD and note that the particles that are to fill this shell came from shells crossing the equator at noon over the range 7.4 to 9.7 R_E. The corresponding fluxes at the various pitch angles can be obtained from the PAD's in Figure 5 transformed to the equator and interpolated. (Note that the negative radial Flux gradients, exemplified in Figure 4, Figure in the generation of the butterfly PAD.) The results are shown in Figure 7. For comparison with our transformed results we examine the PAD's for September 18 in Figure 8; these data were aquired near midnight on a quiet day. Note that the transformed results compare most favorably with the measurements at 8 to 9 R_E rather than the 7.4 R_E of the transformation. The discrepancy can be attributed to the temporal variations in the particle fluxes between the two days (the PAD's even on the noon meridian depend upon the degree of magnetic activity) and deficiencies in the Mead [1964] model used by Roederer in the calculations.

Magnetopause Shadowing

Magnetopause shadowing is an extreme variation of drift-shell splitting that occurs on the day side of the earth. In the region of the magnetosphere past noon, beyond that contour of constant equatorial B (Figure 2) that maps from the noon magnetopause to local midnight, we find that the drift paths for 90° pitch-angle electrons map back (westward) to the magnetopause. Unless there is a source of electrons at the magnetopause (scattering from other pitch angles can be a source) there will be no 90° fluxes for the PAD under question. It is very easy to

find examples of this in Ogo-5 data, and in Figure 9, left panel, are shown PAD's acquired in the afternoon showing the effect. In actuality the picture presented, in terms of Fairfield [1968] contours of constant equatorial-B, are too simplistic for much of what occurs near noon; in this prespect, note the middle two panels of Figure 9. For this region we consider the electron drift paths in more detail.

Effect of the Dayside Minimum-B Regions

As the electrons drift eastward towards noon in the extended magnetosphere beyond ~9 R_E they may encounter branch points, depending upon equatorial pitch angle, which moves them north or south away from the equator onto new minimum-B surfaces. (Note that in the undistorted magnetosphere the minimum-B surface in the field topology encompasses the equator.) Shabansky [1971] has analyzed the situation and points out that the second invariant is halved at the branch points. The picture we have, then, is a particle bouncing back and forth on field lines threading the minimum-B surface, with one mirror point toward the geomagnetic equator and the other toward the earth. The minimum-B surface moves to its highest latitude near the noon meridian.

The author's colleague, R. M. Buck, has calculated some of these drift effects by means of invariant tracing in a model field after first following detailed particle motion to show that the equator and high-latitude regions are topologically connected; early results were presented at a previous meeting [Buck, 1975]. Figure 10 shows results for the Choe and Beard [1974] magnetic field model. The particles were started 70° away from noon on the equator at equatorial pitch angles of 70, 75, 80, and 85° at radial distances of 9.5, 10, 11 and 12 R_E. Particles near 90° pitch angles drift to the magnetopause to be lost as described under "magnetopause shadowing," and those with equatorial pitch angles less than 65° drift through noon well inside the magnetosphere.

Figure 10 shows only the near-magnetopause mirror points of the respective particle groups. Here we note that for 9.5 and 10 R_E, the 70° pitch-angle particles are mirroring close to but just inside the magnetopause, whereas for 11 and 12 R_E, the 70° particles do not reach this point in space having encountered the magnetopause earlier. This all means that these particles are scattered preferentially by encounters with the wave-rich region near the magnetopause and are lost from our distribution of drifting particles whereas the 85° pitch-angle particles are subject to less scatter.

Confirmation of these ideas comes from examining equatorial PAD's in the afternoon magnetosphere after the various drift shells have reassembled. Some striking results are shown in Figure 9, center two panels. Near the magnetopause we see simple magnetopause shadowing as discussed earlier, but inward a bit we find PAD's with minima near 65° as predicted by our model. Figure 11 shows a radial profile of the different pitch-angle groups for the data on this day. The extent of the region in which $j_\parallel$ (shown here as j_{50}, the flux at 50° pitch angles) is greater than $j_\perp$ increases as we examine radial data acquired later and later in the afternoon magnetosphere. The region of crossover, $j_\perp = j_\parallel$, follows roughly that constant-B contour which maps from the noon magnetopause to midnight (see Figure 2).

PAD's Near Dusk

Figure 12 shows a radial profile of data acquired near dusk on November 29, 1968, a particularly quiet day magnetically (designated a QQ day). Here we have plots of the perpendicular flux $j_\perp$ and the $j_\parallel$ flux, which is the peak flux at small pitch angles (20 to 40°). One notes the gradual increase in $J_\perp$ relative to $j_\parallel$ as we approach the smaller radial distances including the energy-dependent crossover from $j_\parallel$ to $j_\perp$ at 6 to 8 R_E.

Figure 13 shows data in marked contrast to that of Figure 12. Here we see data acquired on November 3, 1968, two days after the most disturbed period of 1968. Kp at this time was 5^-. Here each data point is plotted for 4.6-sec acquisition times as the experiment scanned back and forth at 3°/sec. The upper and lower envelopes of the data correspond to $j_\parallel$ (the peak flux at 20 to 40°) and $j_\perp$. To provide the right perspective, proton data, 100-150 keV, are included; the protons have drifted through the nighttime magnetosphere not subject to the violent magnetic activity that occurred for the electrons near the magnetopause. The outer boundary of the protons is at ~16.9 R_E which corresponds to the magnetopause in agreement with the magnetometer data.

In examining the electron data, in particular the lowest energy channel, we find that the $j_\perp$ fluxes show far greater temporal fluctuations than do the $j_\parallel$ fluxes. This is vivid proof that the $j_\perp$ fluxes were closer to the magnetopause during their drift through noon than were the $j_\parallel$ fluxes. Another interesting facet of the data is that beyond ~15.2 R_E, the $j_\parallel$ fluxes as well as $j_\perp$ fluxes, are wiped out. We expect the $j_\perp$ fluxes to be gone but it takes pronounced temporal changes in the field configuration to wipe out the $j_\parallel$ fluxes as well.

Premidnight Magnetosphere

Let us proceed azimuthally into the nighttime magnetosphere in our examination of data. Figure 14 shows a radial profile of the $j_\perp$ and $j_\parallel$ fluxes for October 21, 1968, and Figure 15 shows corresponding PAD's for the lowest energy channel (79 keV) of the LLL Ogo-5 spectrometer. Here we find that the effects of drift-shell splitting are very strong. This was an especially quiet day magnetically ($Kp = 0^+$). In Figure 16 we show a second example of quiettime data. These data were acquired on September 18, 1968, when Ogo 5 was inbound 1 to 2 hours before midnight during a very quiet time magnetically ($Kp = 1^-$). The corresponding PAD's were presented earlier in Figure 8. So far we have shown only quiettime data in the nighttime magnetosphere. However, even during substorms the butterfly PAD is seen in this region of space for all but ~30 min before onset and ~10-15 min after onset. During these periods isotropy usually prevails. Such quiettime data in this part of the magnetosphere is not the norm, more often being punctuated by a substorm or two on such an inbound pass. However, we now examine the results of a modeling study of quiettime data acquired in the midnight meridian before proceeding to substorm effects.

PAD's Near Midnight — Quiettime Modeling Study

On a number of Ogo-5 inbound passes near midnight during quiettimes the PAD's of the particles when first observed were isotropic which were

followed by the rigidity-dependent transition to the butterfly PAD nearer the earth. The low-rigidity particles made the transition first followed in turn by the higher rigidity particles. Figures 17 and 18 show two extremes in the data acquired near midnight during quiet times [West et al., 1978ab] (the August-2 data were acquired during a period of enhanced dynamic pressure [West et al., 1978a] which may account for the difference between the August-2 and -25 data). For each figure the top panel shows the Ogo-5 magnetic field data in GSM coordinates, measured by the UCLA experiment; the middle panel shows the scan-modulated data (plotted every 4.6 sec), obtained by the LLL experiment on Ogo 5; and, the bottom panel shows a rough sketch of the field configuration inferred from the data. The August-2 data strikingly show the point to be made and that is in the region of sharpest curvature along the field line (neutral sheet) that for the particle motion to be adiabatic (conservation of first and second invariants, μ and J) we need the maximum gyroradius of the electrons to be less than ~1/10 the minimum radius of curvature of the guiding field line, or stated differently, less than 1/10 of B_z divided by the gradient of B in the neutral sheet [Alfvén and Fälthammer, 1963]. The details of the particle motion in the region of the neutral sheet have been discussed by Speiser [1967], Shabansky [1971], Sonnerup [1971] and Eastwood [1972]. The transition in the scan modulation of the August-2 data at 0634 UT is the dividing line between μ-J breakdown in the neutral sheet for trajectories on field lines farther from the earth and μ-J conservation for trajectories on field lines closer to the earth. On this particular day we were able to identify the transition points for electrons in five channels, 79 to 822 keV, and protons in two channels, 100-570 keV. In contrast, we note that for the August-25 data the point of μ-J violation for the 79-keV electrons was much farther from the earth than for August 2. The pitch angle changes in conjunction with the UCLA magnetic field data were used in a modeling study [West et al., 1978b]. It was possible to find a model which fits both aspects of the data quite well, that is the particle pitch-angle changes and magnetic field values. Particle motion in the model field was then studied and the results give insight to the structure of the plasma sheet.

These findings enhance earlier results at low altitudes near the trapping boundary. For example, Fritz [1968] has noted a region of isotropy near midnight even during quiet times. Imhof et al. [1977] have made detailed PAD measurements at low altitudes near midnight showing profiles of rigidity-dependent transitions to isotropy, being highest in rigidity at lower L-shells as expected from our modeling study. The profiles were acquired at a variety of magnetic activity levels, Kp = 2 to 5^+. In general, the higher the activity the lower in L-shell was the measured transition point, showing that the field was more taillike for these cases as expected.

PAD's at 6.6 to 15 R_E During Substorms Near the Midnight Meridian

The PAD of energetic electrons drifting into the region at 9 to 19 R_E (as observed on Ogo-5) near midnight during quiettimes ranges from isotropic to butterfly. At 9 R_E, almost without exception, we find the butterfly PAD whereas at the greater distances, depending upon just how taillike the field is, we may find that the isotropic

PAD prevails. The concepts governing the changeover in observed PAD during quiettimes were discussed earlier.

At times, dynamic changes in the field configuration can dominate the azimuthal effects that the electrons are subject to during their drift. In plasma-sheet observations in the near-magnetotail, copious quantities of energetic electrons and protons are almost always found. Usually, in the period of a half hour or so before a substorm expansion or onset, the magnetic field is observed to become more taillike. Proof that the field rotation observed only at the satellite truly results in a more taillike field over a large region of the magnetosphere comes from the fact that Ogo-5 observations show repeated examples of the transition from the butterfly PAD to isotropy during these growth-phase periods. Some of these effects are shown in Figure 19 taken from [Pytte and West, 1978]. Here we see substorm expansion phases as marked at 1701, 1933, 2011, 2252, and 0105 UT. Onset was determined primarily by Pi 2 micropulsations, and all but the onset at 1933 UT are readily apparent in the Ogo-5 particle and field data. The effects between 2011 and 2252 UT are especially interesting. Following onset at 2011 UT the field became more dipolelike. Initially at onset, and this is always the case, the PAD's were isotropic but then on the time scale of minutes the butterfly PAD gradually reemerged, first at the higher energies (not shown) and later the lower energies. Kivelson et al. [1973] attribute this time dispersion to the drift of the electrons from an undisturbed region of the magnetosphere. The reemergence of the butterfly PAD during the expansion is vivid proof that the field configuration, at least to the west, had become more dipolelike than that which prevailed earlier. A southward turning of the IMF reached the magnetopause at ~2155 UT signaling the start of a new growth phase. Possibly the normal recovery of the magnetosphere to a more taillike field may have meant the loss of the butterfly PAD at Ogo 5. In any respect, the new growth phase hastened the change of the PAD to isotropy which was accompanied by the observation of electron-precipitation bremsstrahlung at balloon altitudes in Scandinavia. During the next expansion phase, after 2252 UT, the field never became dipolelike enough and/or long enough to allow the butterfly PAD to emerge. Although not too obvious in the data presented here (observational reasons), the butterfly PAD did reemerge after the 0105-UT expansion. Further examples of substorm related PAD changes observed on Ogo-5 are reported in West et al. [1973b], Pytte and West [1978] and Pytte et al. [1976].

Baker et al. [1978] have made repeated observations of PAD's of electrons ~30 keV at synchronous orbit in the nighttime sector during substorms. During quiettimes the normal PAD was observed, but almost without exception the butterfly PAD was observed during the growth to a more taillike field configuration in the period prior to substorm onset. At onset, the normal PAD returned. Some aspects of these observations were reported previously by Bogott and Moser [1971]. The transition from the normal distribution to the butterfly PAD during the growth phase is marked evidence of the appearance of more taillike fields. The concepts have been discussed earlier. We need the concept of drift-shell splitting coupled with a negative radial gradients in the electron fluxes. Although relatively smooth negative radial gradients

often exist, the flux change may be more drastic than that. Quite often, we expect, that during substorm growth phases the field distortions and inward motion of the magnetopause are such that magnetopause shadowing exists for the equatorially mirroring electrons as described in a previous section. In such cases the drift paths of these electrons map westward to the magnetopause along contours of constant B so that only electrons of smaller equatorial pitch angles are seen near midnight.

In Figure 20, top panel, we have provided a summary sketch for the ideas presented in this section. (The reader may wish to refer to Pytte and West [1978] and West et al. [1978a] for further discussion of these ideas.) The top panel shows the situation that prevails for the data of Baker et al. [1978], the bottom two panels show the contrasting situation at Ogo-5. In the top panel we note that prior to substorm thinning the normal PAD prevails, which gives way to the butterfly PAD during substorm thinning. In the second panel we find the butterfly PAD during quiet times, which gives way to isotropy during thinning and early expansion. In the bottom panel, at the more extended distances, note that it is probable that the isotropic PAD prevails presubstorm because taillike fields usually prevail. Here the butterfly PAD is expected only for a period during recovery when the field is dipolelike enough to support adiabatic guiding center motion.

Post Midnight — 9 to 15 R_E

The PAD found at roughly 9 to 15 R_E past midnight to near dusk tends toward isotropy (however, in many cases the PAD we observe may have a loss cone but we cannot tell) but quite often the butterfly effect is observed. We have already discussed the effects that occur near midnight during both quiet and disturbed periods. During very quiet periods, probably accompanied by low dynamic-pressure of the solar wind with small or northward IMF, we can expect the electrons to drift through midnight still maintaining a marked butterfly PAD. However, we noted that often during very quiet times, probably in association with enhanced dynamic pressure in the solar wind, that the field configuration could be taillike enough to cause isotropy. Conversely during substorms, beyond 8 to 9 R_E, we found isotropy during the growth and early expansion phases followed by the emergence of the butterfly PAD during the times of the more dipolar fields.

Although much is known about how the PAD's evolve as they drift through midnight, we do not have all of the answers. Figure 21 shows a radial profile of scan-modulated electron fluxes obtained on an inbound pass of Ogo-5 near dawn on June 5, 1968, a very quiet time magnetically ($Kp = 1^+$). The PAD forms are sketched on the figure. Figure 22 shows detailed PAD's obtained on this pass. Here we find periods of isotropy interspersed with the butterfly PAD. Such distributions of PAD's are common in this region of the magnetosphere. However, note that the flux at 90° is markedly enhanced relative to that observed just past dusk, Figure 15, in an equivalent region premidnight. It is very possible that other mechanisms not previously mentioned are operative. Assume for the moment that the electrons become isotropic due to the necked-down field configuration near midnight but only moments later in their azimuthal drift are back on field lines allowing

μ-J conservation. At this point, assuming that the particle motion is still taking place in the plasma sheet, we find that we have electrons near 90° pitch angles drifting faster than those at low pitch angles [e.g., West et al., 1978b]. The production rate is proportional to the drift rate of electrons at low pitch angles into the isotropizing region, and here we have a situation which can lead to the evolution of the butterfly effect in an hour or so of azimuthal drift. However, this does not usually lead to the very low values of $j_\perp$ relative to $j_\parallel$ seen premidnight. In addition, for the lower energies we expect that electric fields in the nighttime magnetosphere are contributing somewhat to modification of the PAD's.

Proton and Proton-Electron Associated Observations

General

Most of the pitch-angle effects seen in the PAD's of energetic electrons in the equatorial magnetosphere have been seen also for energetic protons. For example, the butterfly effect has been seen at 6.6 R_E by Stevens et al. [1970] and Bogott and Mozer [1971]. The LLL Ogo-5 PAD observations at 100-150 keV show the combined effects of spatial gradients, the butterfly effect, and breakdown of adiabatic guiding-center motion. There have been case studies of these PAD's but no systemmatic studies. However, it can be clearly stated that the butterfly PAD exists across the nighttime magnetosphere, but even on quiet days isotrophy exists (occurs when the gyro radii of the protons are greater than ~1/10 the minimum curvature of the field lines) much beyond 8 R_E. In the inner magnetosphere the normal PAD exists and the effects there are documented by, e.g. Williams and Lyons [1974]. In the morning magnetosphere at, say, 9 R_E we might expect to see the effects of magnetopause shadowing. All too often the protons studied from Ogo-5 data had gyro radii that were too large to allow traversal of the minimum-B regions without scattering. Nevertheless, we have made observations of proton PAD's on disturbed days, that is with a contracted magnetopause, in which PAD's similar to the center panel of Figure 9 were observed. There was one major difference, however, and that is a strong component of isotropy (near 0 and 180°) existed in conjunction with the PAD. A strong component of isotropy appears to be the norm in the PAD's of energetic protons in the extended regions on the dayside of the earth.

Region of the Magnetopause

The transition from magnetosheath to magnetosphere is usually signaled by the change in the field orientation and noise and by changes in the plasma-flow pattern. Quite as specific though is the appearance of a double loss cone in the PAD's of the energetic electrons and protons, the electron data being most easily interpreted. Figure 23 shows an example of an Ogo-5 magnetopause crossing near noon. The electron and proton data from the LLL experiment are plotted every 4.6 sec as the experiment scanned back and forth at 3°/sec. The zigzag pattern at the top of the figure is the instantaneous pitch angle of the particles read from the scale to the right. For perspective note that peaks in the electron counting rate are at 90°.

From the magnetometer we note the magnetopause crossing at 0837 UT. The spikes in the proton data prior to that are the signatures of flowing sheath protons [West and Buck, 1976; Roelof et al., 1976]. The data are consistent with momentary return to the sheath at ~0846 and 0851 UT.

In this pass the signature of the transition from sheath to magnetosphere is relatively clear. However, at high latitudes and along the flanks of the magnetosphere, where the boundary layer is relatively thick, the transition is not always obvious. This is especially the case when appreciable fluxes of protons and electrons are observed flowing downstream in the magnetosheath. Particularly good examples of the situation under discussion are to be found in Figures 3 and 4 of West and Buck [1976] showing data acquired on satellite passes near dusk.

Energetic-Proton Spatial Gradients and the East-West Effect

The gyro radius of 100-150 keV protons in a 50-γ field is 0.16 R_E, a situation which pertains to the equatorial dayside magnetopause. Measurements of $j_\perp$ from a scanning spectrometer, such as the LLL Ogo-5 experiment, show asymmetries in the data that are due to the fact that with the spectrometer looking westward it measures protons with gyro centers 0.16 R_E farther from the earth than the radial position of the spacecraft and when looking eastward measures protons with gyro centers 0.16 R_E closer to the earth, a range of 0.32 R_E. Appreciable proton flux gradients can occur over this distance, and thus from a single point in space one can obtain a snapshot of the particle distribution. The geometry of this situation is shown in Figure 24. Kaufman and Konradi [1973] have taken advantage of such effects in studying magnetopause boundary motions. Also, Kaufman et al. [1972] have studied field-line motions at L = 5 at high latitudes on the nightside of the earth during a magnetic storm. Recently Williams [1978] has analyzed early Isee results using three-dimensional data from his scanning proton spectrometer. His paper touches on aspects of the previous section as well as the east-west effect.

We have taken advantage of the east-west effect during the growth phase of a substorm [Buck et al., 1973] to study the motion of the plasma sheet in the near magnetotail. In this situation the partical fluxes fall off north and south of the plasma sheet and in a very real sense the particle intensities reflect the field configuration. Figure 25 provides the picture. The upper panel shows typical proton orbits at the edge of the plasma sheet. The Ogo-5 spectrometer measured these protons by scanning in the plane perpendicular to the earth's radius vector. (Note that the geometry of Figure 24 is idealized; for the case in hand the scan plan is at a marked angle with respect to $\vec{B}$.) Since the protons were intrinsically isotropic we were able to use data at all pitch angles which were then ordered in terms of the distance of the gyro centers from the neutral sheet. These results are shown in the lower panel as proton flux profiles at different times. Note that Z_B is the perpendicular distance from $\vec{B}$ at the time of onset of substorm thinning, 0641 UT. The velocity of thinning of the edge of the plasma sheet was inferred from these data [cf. Buck et al., 1973].

Vela experimenters [Palmer et al., 1976] have employed a similar analysis in the lobes of the magnetotail. They used proton spatial gradients measured during a solar particle event to provide the first measurement of field line motions high in the lobes of the magnetotail. Obviously the proton east-west effect is a very powerful tool, especially when one is limited to only one satellite in making observations.

Energetic Proton and Electron Flow in the Magnetotail

In the last section we made use of the gradients of the particle fluxes to determine boundary motions. Here we discuss a different feature in the proton fluxes, the Compton-Getting effect, which is important when the center-of-flow motion is appreciable in respect to particle velocities. Here the observer sees particles increased in energy when looking upstream and decreased in energy when looking downstream. As a result, an anisotropy appears in the directional distributions if the energy spectra decrease sufficiently rapid with increasing energy. Historically, field line motion in the magnetotail has been measured by means of low-energy plasma observations, of course, taking advantage of the Compton-Getting effect. Interestingly though, energetic protons can provide such measurements. Recently Roelof et al. [1976] and Keath et al. [1976] have used data from the 16-sector 50-200-keV proton spectrometer on Imp 7 for such measurements at 35 R_E down the tail. Well-defined anisotropies during substorms were observed which are readily interpreted as a flow. These data support the current idea of the formation of an X-type neutral line and its attendant motions.

Baker and Stone [1976] have made measurements of >200-keV electrons using their 8-sector scanning spectrometer on Imp 8 at ~30 R_E in the magnetotail. Unlike protons the Compton-Getting effect causes very little anisotropy in the counting rates of energetic electrons since the velocities of the electrons are large compared to the flow velocities. Normally the PAD's are isotropic or on occasion show the butterfly PAD. However, Baker and Stone have observed asymmetries in the PAD's of the electrons which are associated with substorms. During substorms they have observed streaming away from the earth suggestive of an X-type neutral line between the satellite and earth and that the observations were being made on open field lines.

Conclusions

Clearly the PAD's of energetic particles that we have been discussing can be used as excellent diagnostic tools in the study of field configurations. Although much of what was presented was qualitative, in most cases the underlying theory is well known. Obviously the routine use of PAD data as discussed here, but on a more quantitative basis, is very important in our future studies of magnetospheric structure.

Acknowledgments. I would like to thank those colleagues who have worked the most closely with me in the Ogo-5 researches, my immediate colleague R. M. Buck, M. G. Kivelson from UCLA, and T. Pytte from the

University of Bergen. I am especially grateful to the UCLA magnetometer experimenters, P. J. Coleman and C. T. Russell, for the ready availability of good magnetic field data. These field data were essential to the interpretation of the Ogo-5 particle data presented in this review. This work was performed under the auspices of the U. S. Department of Energy by the Lawrence Livermore Laboratory under contract No. W-7405-Eng-48.

References

Alfvén, A., and C. G. Fälthammer, Cosmical Electrodynamics, Fundamental Principles, 2nd edition, Clarendon, Oxford, 1963.

Baker, D. N., and E. C. Stone, Energetic electron anisotropies in the magnetotail: Identification of open and closed field lines, Geophys. Res. Letters, 3, 557, 1976.

Baker, D. N., P. R. Higbie, E. W. Hones, and R. D. Belian, >30-keV electron anistropies at 6.6 R_E as precursors to substorms, EOS Trans. Amer. Geophys. Union, 59, 357, 1978. Submitted to Geophys. Res. Letters, 1978.

Bogott, F. H., and F. S. Mozer, Equatorial electron angular distributions in the loss-cone and at large angles, J. Geophys. Res., 76, 6790, 1971.

Buck, R. M., H. I. West, Jr., and R. G. D'Arcy, Jr., Satellite studies of magnetospheric substorms on August 15, 1968: Ogo-5 energetic proton observations-spatial boundaries, J. Geophys. Res., 78, 3103, 1973.

Buck, R. M., Energetic electron drift motions in the outer dayside magnetosphere — observations and calculations, EOS Trans. Amer. Geophys. Union, 56, 628, 1975.

Choe, J. Y., and D. B. Beard, The compressed geomagnetic field as a function of dipole tilt, Planet. Space Sci., 22, 595, 1974.

Eastwood, J. W., Consistency of fields and particle motion in the 'Speiser' model of the current sheet, Planet. Space Sci., 20, 1555, 1972.

Fairfield, D. H., Average magnetic field configuration of the outer magnetosphere, J. Geophys. Res., 73, 7329, 1968.

Fritz, T. A., High-latitude outer-zone boundary region for ≥40-keV electrons during geomagnetically quiet periods, J. Geophys. Res., 73, 7245, 1968.

Haskell, G. P., Anisotropic fluxes of energetic particles in the outer magnetosphere, J. Geophys. Res., 74, 1940, 1969.

Imhof, W. L., J. B. Reagan, and E. E. Gaines, Fine-scale spatial structure in the pitch-angle distributions of energetic particles near the midnight trapping boundary, J. Geophys. Res., 82, 5215, 1977.

Kaufman, R. L., and A. Konradi, Speed and thickness of the magnetopause, J. Geophys. Res., 78, 6549, 1973.

Kaufman, R. L., J. T. Horng, and A. Konradi, Trapping boundary and field-line motion during geomagnetic storms, J. Geophys. Res., 77, 2780, 1972.

Keath, E. P., E. C. Roelof, C. O. Bostrom, and D. J. Williams, Fluxes of ≥50-keV protons and ≥30-keV electrons at ~35 R_E: 2. Morphology and flow patterns in the magnetotail, J. Geophys. Res., 81, 2315, 1976.

Kivelson, M. G., M. P. Aubry, and T. A. Farley, Satellite studies of magnetospheric substorms on August 15, 1968, 5. Ogo-5 energetic electron observations: spatial boundaries and wave-particle interactions, J. Geophys. Res., 78, 3079, 1973.

Lyons, L. R., R. M. Thorne, and C. S. Kennel, Pitch angle diffusion of radiation belt electrons within the plasmasphere, J. Geophys. Res., 77, 3455, 1972.

Lyons, L. R., and D. J. Williams, The quiet time structure of energetic (35-560 keV) radiation belt electrons, J. Geophys. Res., 80, 943, 1975.

Mead, G. D., Deformation of the geomagnetic field by the solar wind, J. Geophys. Res., 69, 1184, 1964.

Northrop, T. G., and E. Teller, Stability of the adiabatic motion of charged particles in the earth's field, Phys. Rev., 117, 215, 1960.

Palmer, I. D., P. R. Higbie, and E. W. Hones, Jr., Gradients of solar protons in the high-latitude magnetotail and the magnetospheric electron field, J. Geophys. Res., 81, 562, 1976.

Pytte, T., R. L. McPherron, M. G. Kivelson, H. I. West, Jr., and E. W. Hones, Jr., Multiple-satellite studies of magnetospheric substorms: radial dynamics of the plasma sheet, J. Geophys. Res., 81, 5921, 1976.

Pytte, T., and H. I. West, Jr., Ground-satellite correlations during presubstorm magnetic field changes and plasma sheet thinning in the near-earth magnetotail, J. Geophys. Res., 83, 3791, 1978.

Roederer, J. G., On the adiabatic motion of energetic particles in a model magnetosphere, J. Geophys. Res., 72, 981, 1967.

Roelof, E. C., E. P. Keath, C. O. Bostrom, and D. J. Williams, Fluxes of $\geq$50-keV protons and $\geq$30-keV electrons at ~35 R_E: 1. Velocity anisotropies and plasma flow in the magnetotail, J. Geophys. Res., 81, 2304, 1976.

Schultz, M., Drift-shell splitting at arbitrary pitch angle, J. Geophys. Res., 77, 624, 1972.

Serlimitsos, P., Low energy electrons in the dark magnetosphere, J. Geophys. Res., 71, 61, 1966.

Shabansky, V. P., Some processes in the magnetosphere, Space Sci. Rev., 12, 299, 1971.

Sonnerup, B. U. O., Adiabatic particle orbits in a magnetic null sheet, J. Geophys. Res., 76, 8211, 1971.

Speiser, T. W., Particle motion in model current sheets, 2. Applications to auroras using a geomagnetic tail model, J. Geophys. Res., 72, 3919, 1967.

Stevens, J. R., E. F. Martina, and R. S. White, Proton energy distributions from 0.060 to 3.3 MeV at 6.6 earth radii, J. Geophys. Res., 75, 5373, 1970.

West, H. I., Jr., R. M. Buck, and J. R. Walton, Electron pitch angle distributions throughout the magnetosphere as observed on Ogo-5, J. Geophys. Res., 78, 1064, 1973a.

West, H. I., Jr., R. M. Buck, and J. R. Walton, Satellite studies of magnetospheric substorms on August 15, 1968: 6. Ogo 5 energetic electron observations — pitch angle distributions in the nighttime magnetosphere, J. Geophys. Res., 78, 3093, 1973b.

West, H. I., Jr., and R. M. Buck, Pitch angle distributions of energetic electrons in the equatorial regions of the outer magnetosphere — Ogo 5 observations, in Magnetospheric Physics, edited by B. M. McCormac and D. Reidel, p. 93, Dordrecht-Holland, 1974.

West, H. I., Jr., and R. M. Buck, Observations of >100-keV protons in the earth's magnetosheath, J. Geophys. Res., 81, 569, 1976.

West, H. I., Jr., R. M. Buck, and M. G. Kivelson, On the configuration of the magnetotail during quiet and weakly disturbed periods: State of the magnetosphere, J. Geophys. Res., 83, 3805, 1978a.

West, H. I., Jr., R. M. Buck, and M. G. Kivelson, On the configuration of the magnetotail near midnight during quiet and weakly disturbed periods: Magnetic field modeling, J. Geophys. Res., 83, 3819, 1978b.

Williams, D. J., and L. R. Lyons, Further aspects of the proton ring current interaction with the plasmapause: Main and recovery phases, J. Geophys. Res., 79, 4791, 1974.

Williams, D. J. (Northern Oceanic and Atmospheric Administration, Boulder, Colorado), unpublished manuscript, 1978.

Figure Captions

Fig. 1. Survey of energetic electron PAD's in the near equatorial magnetosphere as determined by the Lawrence Livermore Laboratory's experiment on Ogo 5.

Fig. 2. Contours of constant B in the equatorial regions for an average magnetosphere [Fairfield, 1968].

Fig. 3. Transformation of drift shells from the dayside to nightside magnetosphere as calculated by Roederer [1967]. The dots in each case represent the mirror points of each particle group as identified by the cosine of the equatorial pitch angle.

Fig. 4. Radial $j_\perp$ profiles of energetic electron fluxes on March 30, 1968, as determined on Ogo 5.

Fig. 5. Energetic electron PAD's measured by Ogo 5 on March 30, 1968.

Fig. 6. Transformation of drift shells from the nightside to dayside magnetosphere as calculated by Roederer [1967]. Conversely, we may use this figure to determine the dayside origins of particles of a given equatorial pitch angle for a particular shell at midnight.

Fig. 7. Ogo-5 March-30 electron PAD data from Figure 5 transformed to midnight by means of Roederer's calculations of drift-shell splitting in Figure 6. The dashes at small angles represent both extrapolations based on the Roederer calculations and the author's expectations based on data.

Fig. 8. Electron PAD's in the quiet nighttime magnetosphere on September 18, 1968, as measured on Ogo 5. These results are presented partially for comparison with the transformed results in Figure 7.

Fig. 9. PAD's of energetic electrons measured near the magnetopause in the early afternoon on January 7, 1969, by Ogo 5.

Fig. 10. Results of following the drift paths of particles of equator pitch angles of 70, 75, 80 and 85° at $\phi_{GSM} = 70°$, started at radial distances of 9.5, 10, 11, and 12 R_E, into the high-latitude minimum-B regions in the noon meridian [Buck, 1975]. The calculations are based on the Choe-Beard field model. The intersections of the grid lines represent the mirror points of the respective particles on the sunward side of the configuration. The conjugate near-earth mirror points are not shown.

Fig. 11. Radial profiles of electron fluxes measured in the early afternoon on January 7, 1969, by Ogo 5.

Fig. 12. Radial profiles of electron fluxes on November 29, 1968, measured on Ogo 5. This was an especially quiet day magnetically ($Kp \approx 1$).

Fig. 13. Radial profiles of electron and proton fluxes on November 3, 1968, measured on Ogo 5. This was a very disturbed day magnetically ($Kp = 5^-$). The electron pitch angle data clearly show the effect of their drift through noon near the fluctuating magnetopause.

Fig. 14. Radial profiles of the electron fluxes on October 21, 1968. This was a very quiet day magnetically ($Kp = 0^+$).

Fig. 15. PAD's of 79-keV electrons in the early evening on October 12, 1968, as measured on Ogo 5.

Fig. 16. Radial profile of the $j_\perp$ and $j_\parallel$ fluxes on September 18, 1968. The $j_\parallel$ fluxes are the peak fluxes at 20 to 40° pitch angles. See Figure 8 for the corresponding PAD's.

Fig. 17. Electron data acquired on an inbound pass of Ogo 5 near midnight on August 2, 1968. The abrupt change in the scan modulation of the 79-keV electrons at 0634 UT is indicative of a change from isotropy to the butterfly PAD. Computer modeling [West et al., 1978b] puts the transition point in the neutral sheet between μ-J breakdown farther and conservation nearer the earth at ~11 R_E. Magnetically August 2 was very quiet ($Kp \approx 1$, a QQ day).

Fig. 18. Electron data acquired on an Ogo-5 inbound pass near midnight on August 25, 1968. Kp was 0^+. Note the scan modulation in the count rates, almost from the first detection of the electrons. Computer modeling [West et al., 1978b] puts the crossover in the neutral sheet between μ-J breakdown farther and conservation nearer the earth at 17 ± 1 R_E. The most obvious difference between this day and that of August 2, Figure 17, is the much higher solar wind dynamic pressure for the latter day.

Fig. 19. Data from a substorm study [Pytte and West, 1978]. The scan modulation (or lack of it) of the Ogo-5 energetic electron data provides a key to the field configuration (see text). Substorm onset as determined by Pi2 micropulsations was at 1701, 1933, 2011, 2252, and 0105 UT as marked.

Fig. 20. Summary diagram showing the PAD's of energetic electrons that can be expected at various distances in the midnight magnetosphere during various phases of substorms. The dot on each Figure is the observation point. Note that field configuration at early expansion is generally believed to be more dipolar than the final field configuration.

Fig. 21. Radial profiles of scan-modulated electron fluxes in the early dawn magnetosphere as measured on Ogo 5 June 5, 1968. Kp was 1^+. The PAD forms are sketched for the various regions.

Fig. 22. PAD's of energetic electrons on June 5, 1968, in the early dawn magnetosphere. See Figure 21 for the corresponding radial profiles. See Figure 16 for PAD's acquired in a roughly equivalent region premidnight.

Fig. 23. Magnetopause crossing on March 17, 1968, into the dayside near-equatorial magnetosphere. The instantaneous pitch angle of the particles being detected is given by the zigzag pattern read from the scale to the right.

Fig. 24. Idealized geometry for observing the proton east-west effect. Here $\hat{\ell}$ refers to the look direction of the experiments aperture which is scanned through θ_s observing protons with gyro radii varying from $Z_B = -\rho$ to $+\rho$. In general the analysis of such scan data must allow for the scan plane being tilted at an appreciable angle relative to $\vec{B}$.

Fig. 25. Use of the proton east-west effect to determine the plasma sheet boundary motions during the 0714-UT August 15, 1968, substorm. The upper panel shows typical proton orbits for 100-150, 230-570, and 570-1350 keV at the edge of the plasma sheet at the position of Ogo 5. The lower panel shows profiles of the proton fluxes at different times inferred from data acquired by the LLL scanning proton spectrometer.

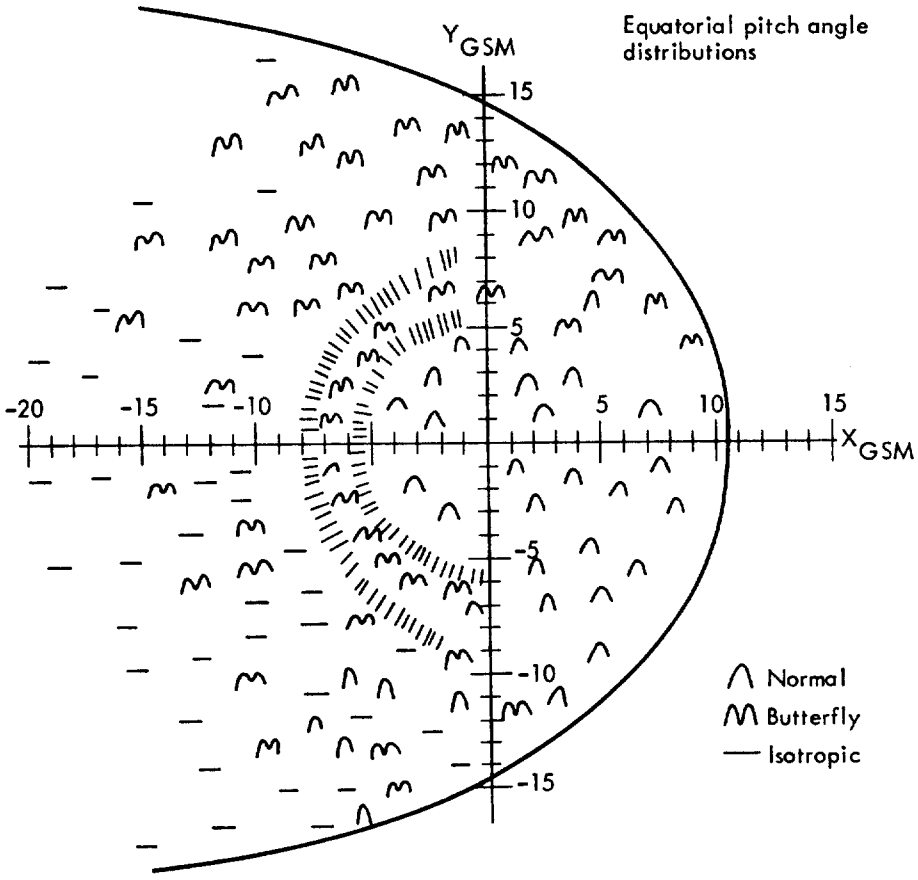
Equatorial pitch angle distributions
Y_{GSM}
15
10
5
-5
-10
-15
-20
-15
-10
5
10
15
X_{GSM}
Normal
Butterfly
Isotropic

West - Fig. 1

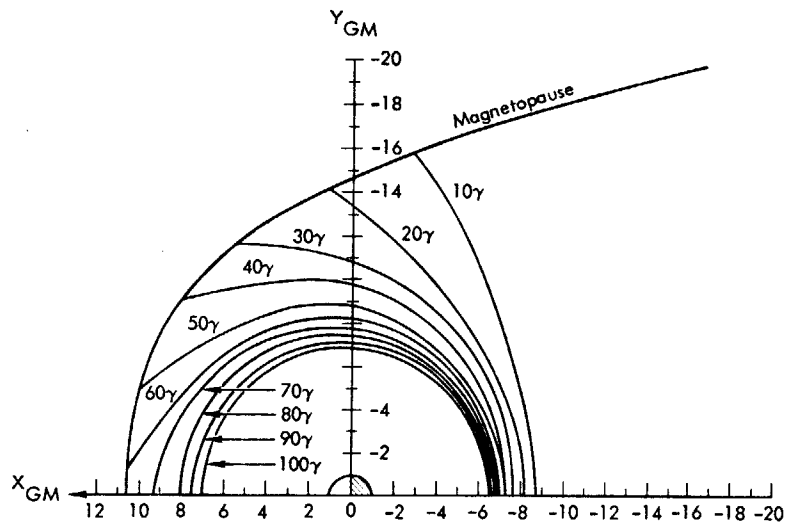
Y_{GM}
-20
-18
-16
-14
-4
-2
Magnetopause
10γ
20γ
30γ
40γ
50γ
60γ
70γ
80γ
90γ
100γ
X_{GM}
12 10 8 6 4 2 0 -2 -4 -6 -8 -10 -12 -14 -16 -18 -20

West - Fig. 2

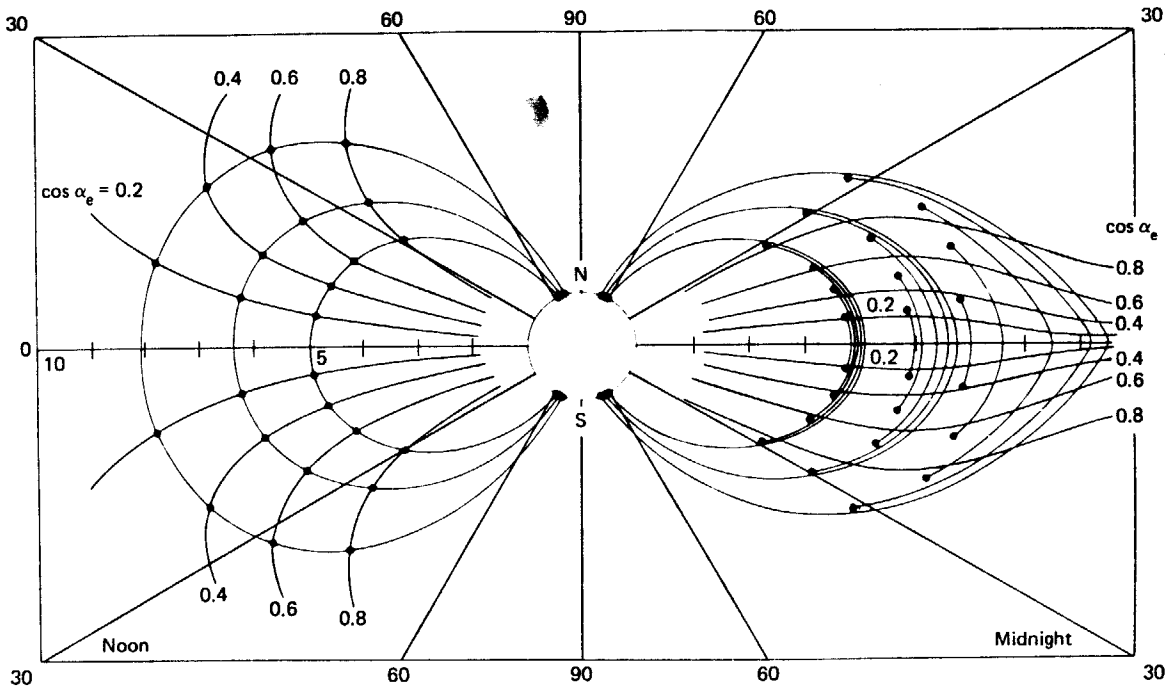
30
60
90
60
30
0.4
0.6
0.8
cos α_e = 0.2
N
0
10
5
S
cos α_e
0.8
0.6
0.4
0.2
0.2
0.4
0.6
0.8
0.4
0.6
0.8
Noon
Midnight
30
60
90
60
30

West - Fig. 3

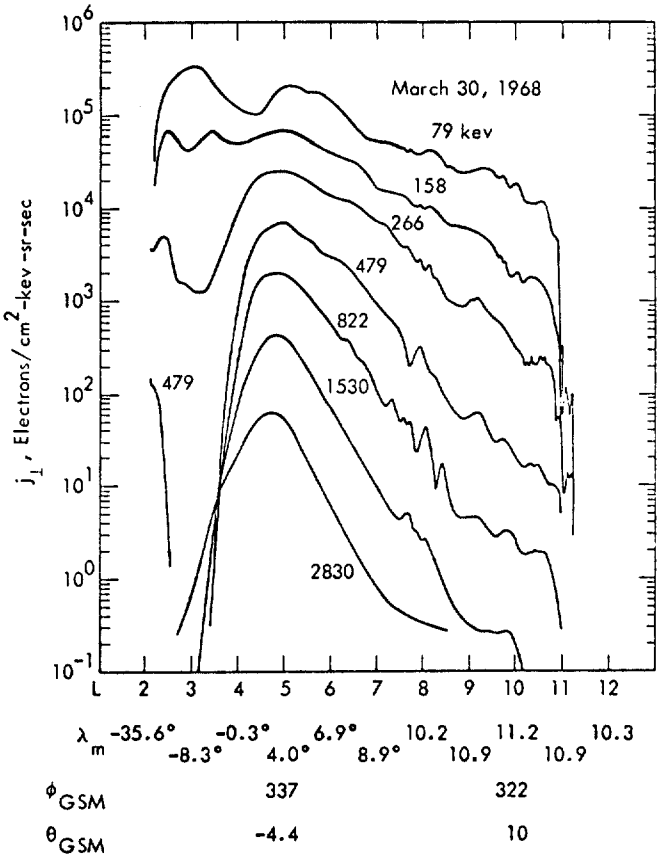
March 30, 1968
79 kev
158
266
479
822
1530
2830
479
$j_\perp$, Electrons/cm^2-kev-sr-sec
L
λ_m
ϕ_{GSM}
θ_{GSM}
-35.6° -0.3° 6.9° 10.2 11.2 10.3
-8.3° 4.0° 8.9° 10.9 10.9
337 322
-4.4 10

West - Fig. 4

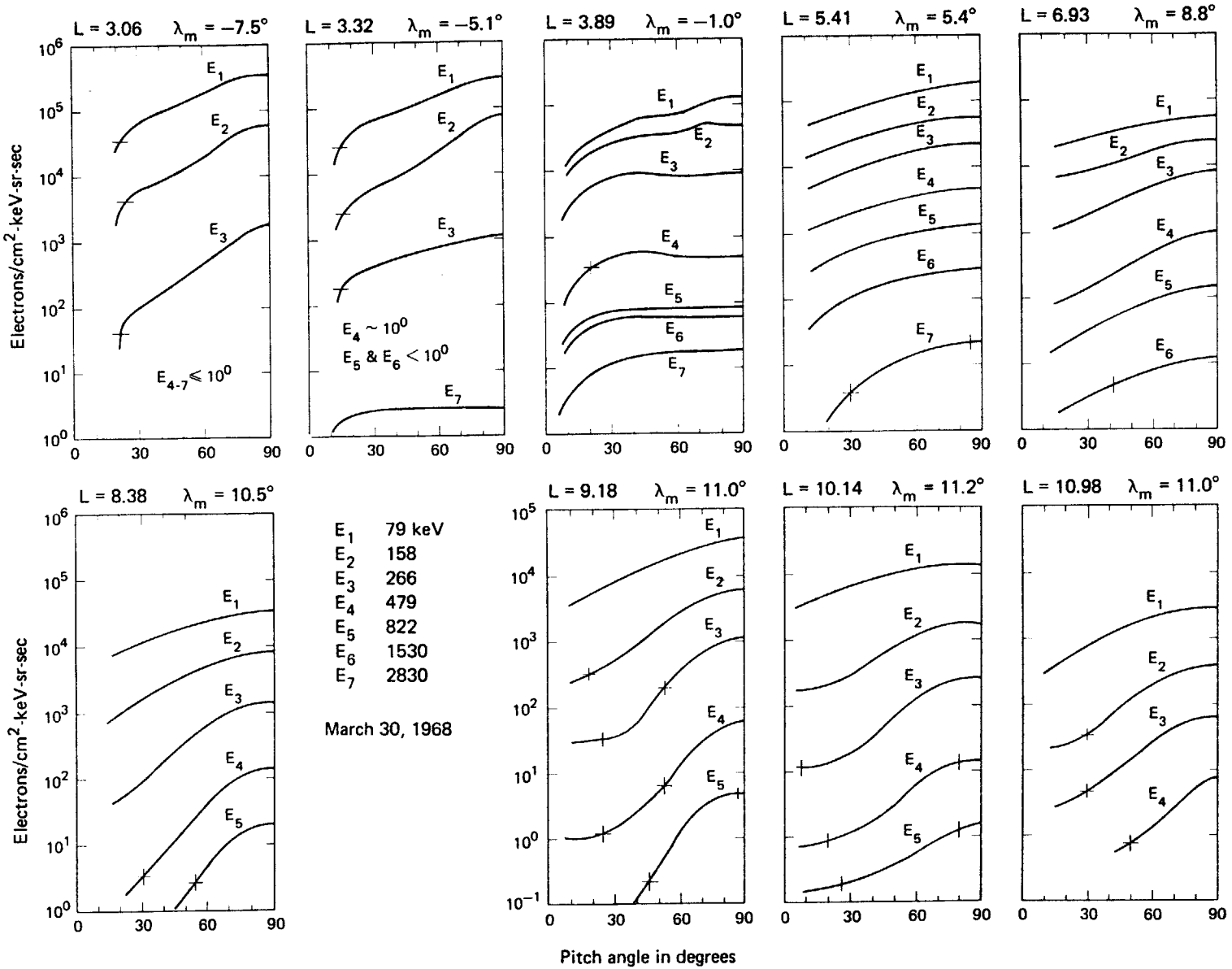
L = 3.06 λm = −7.5°
L = 3.32 λm = −5.1°
L = 3.89 λm = −1.0°
L = 5.41 λm = 5.4°
L = 6.93 λm = 8.8°
L = 8.38 λm = 10.5°
L = 9.18 λm = 11.0°
L = 10.14 λm = 11.2°
L = 10.98 λm = 11.0°
Electrons/cm²-keV-sr-sec
E4-7 ≤ 10⁰
E4 ~ 10⁰
E5 & E6 < 10⁰
E1 79 keV
E2 158
E3 266
E4 479
E5 822
E6 1530
E7 2830
March 30, 1968
Pitch angle in degrees

West - Fig. 5

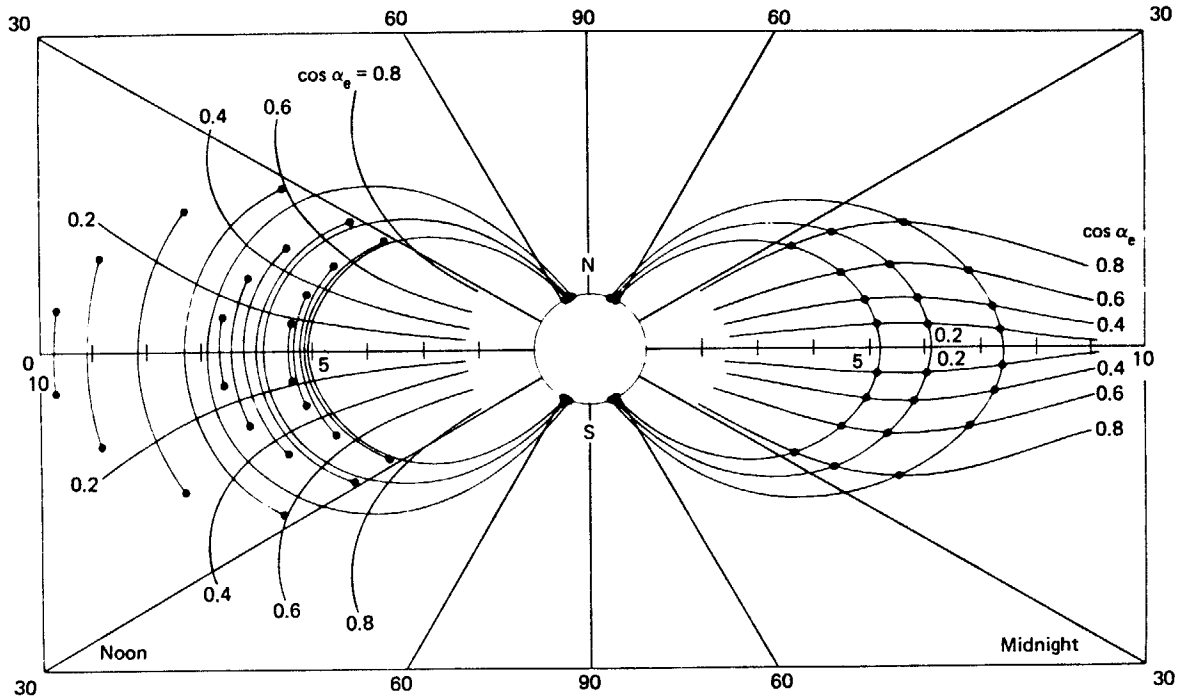
30
60
90
60
30
cos α_e = 0.8
0.4
0.6
0.2
N
cos α_e
0.8
0.6
0.4
0.2
0.2
0.4
0.6
0.8
0
10
5
5
10
0.2
0.4
0.6
0.8
S
Noon
Midnight
30
60
90
60
30

West - Fig. 6

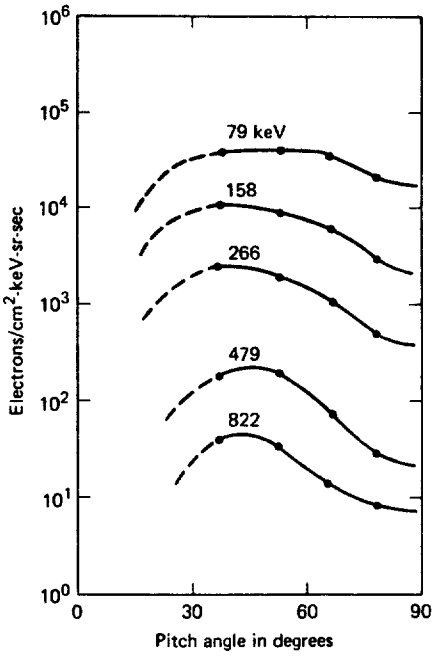
10^6
10^5
10^4
10^3
10^2
10^1
10^0
Electrons/cm^2-keV-sr-sec
79 keV
158
266
479
822
0
30
60
90
Pitch angle in degrees

West - Fig. 7

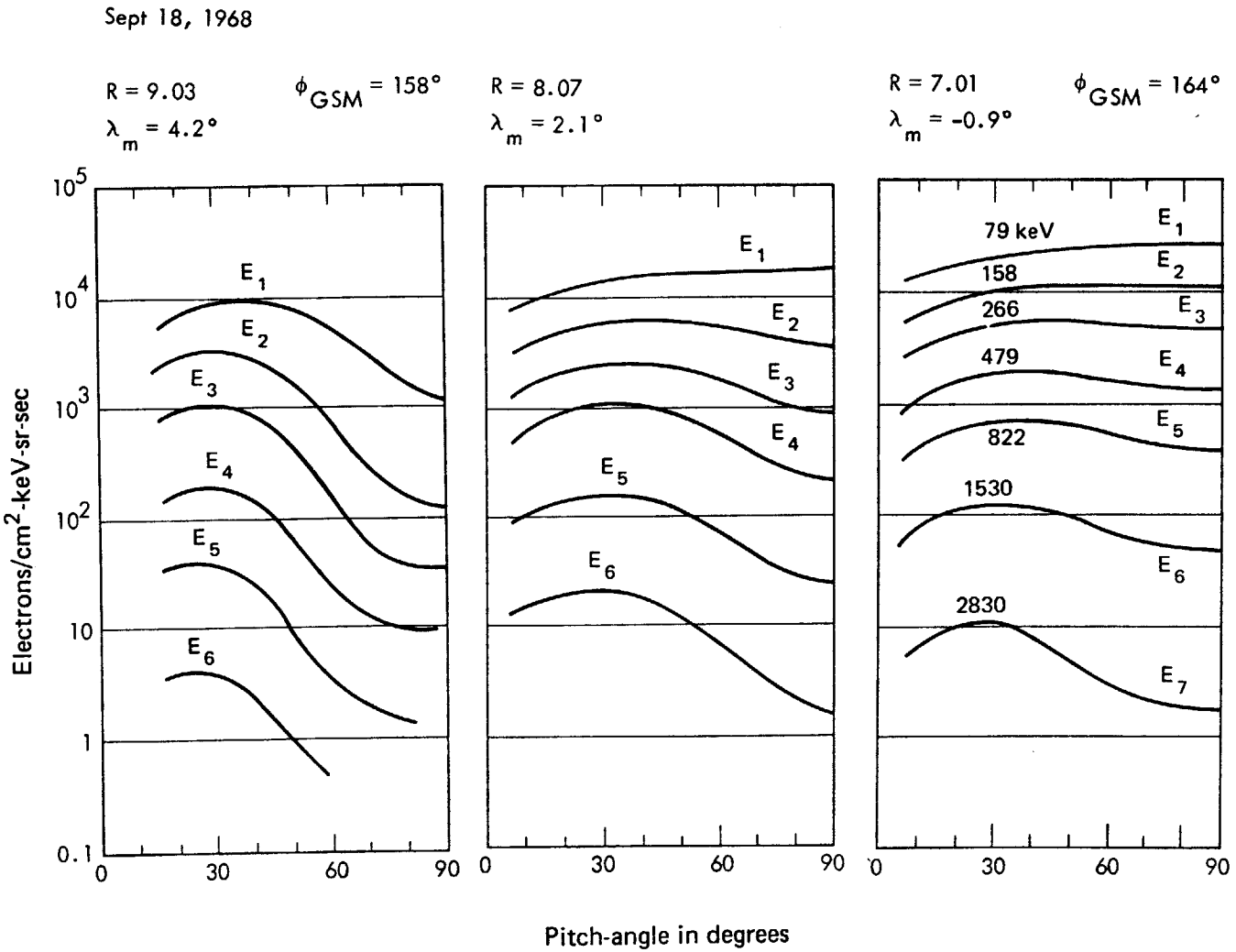
Sept 18, 1968
R = 9.03
λ_m = 4.2°
ϕ_{GSM} = 158°
R = 8.07
λ_m = 2.1°
R = 7.01
λ_m = -0.9°
ϕ_{GSM} = 164°
Electrons/cm^2-keV-sr-sec
10^5
10^4
10^3
10^2
10
1
0.1
E_1
E_2
E_3
E_4
E_5
E_6
79 keV
158
266
479
822
1530
2830
E_7
0
30
60
90
Pitch-angle in degrees

West - Fig. 8

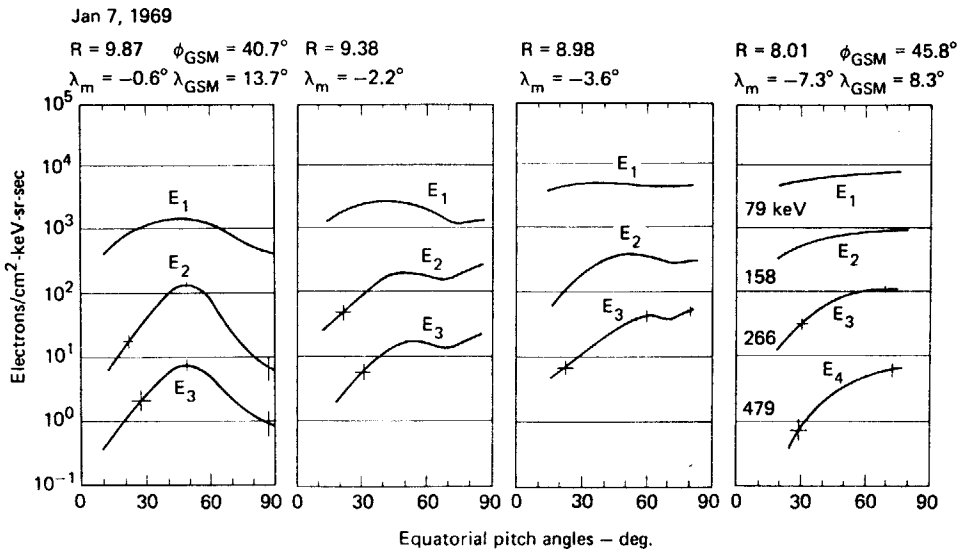
Jan 7, 1969
R = 9.87 ϕ_{GSM} = 40.7° R = 9.38
λ_m = −0.6° λ_{GSM} = 13.7° λ_m = −2.2°
R = 8.98
λ_m = −3.6°
R = 8.01 ϕ_{GSM} = 45.8°
λ_m = −7.3° λ_{GSM} = 8.3°
Electrons/cm²-keV-sr-sec
10^5
10^4
10^3
10^2
10^1
10^0
10^{-1}
E_1
E_2
E_3
E_4
79 keV
158
266
479
0 30 60 90
Equatorial pitch angles — deg.

West - Fig. 9

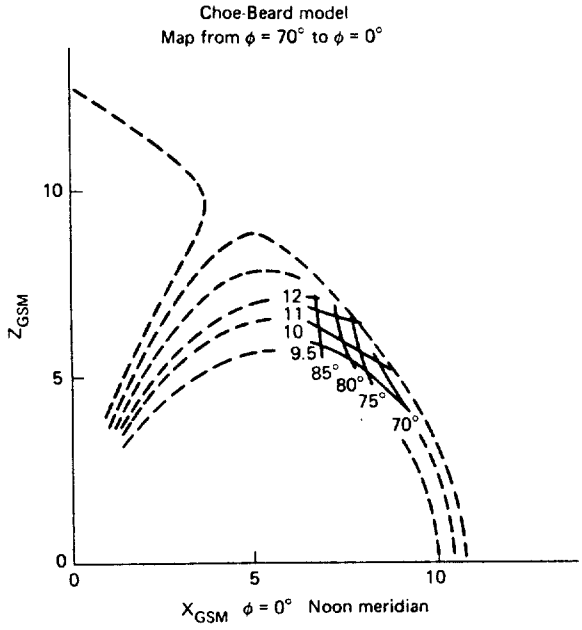
Choe-Beard model
Map from $\phi = 70°$ to $\phi = 0°$
10
5
0
Z_{GSM}
12
11
10
9.5
85°
80°
75°
70°
0
5
10
X_{GSM} $\phi = 0°$ Noon meridian

West - Fig. 10

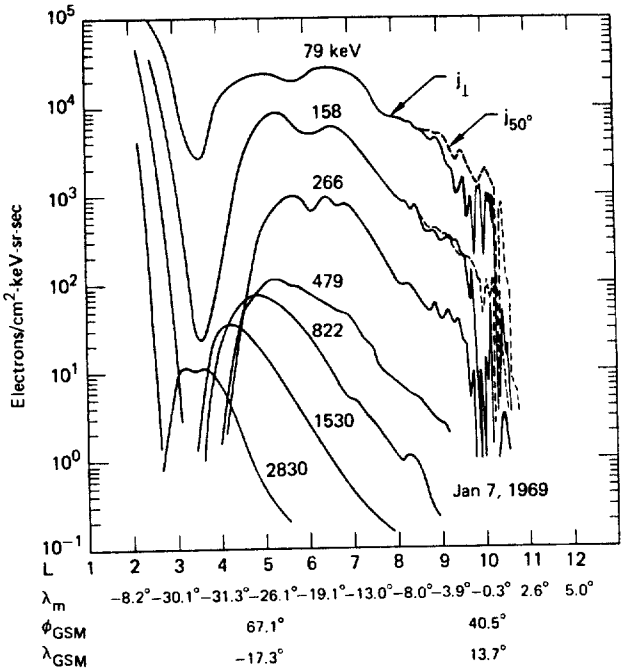
79 keV
158
266
479
822
1530
2830
$i_\perp$
$i_{50°}$
Jan 7, 1969
Electrons/cm²-keV-sr-sec
L
λ_m
ϕ_{GSM}
λ_{GSM}
−8.2° −30.1° −31.3° −26.1° −19.1° −13.0° −8.0° −3.9° −0.3° 2.6° 5.0°
67.1°
40.5°
−17.3°
13.7°

West - Fig. 11

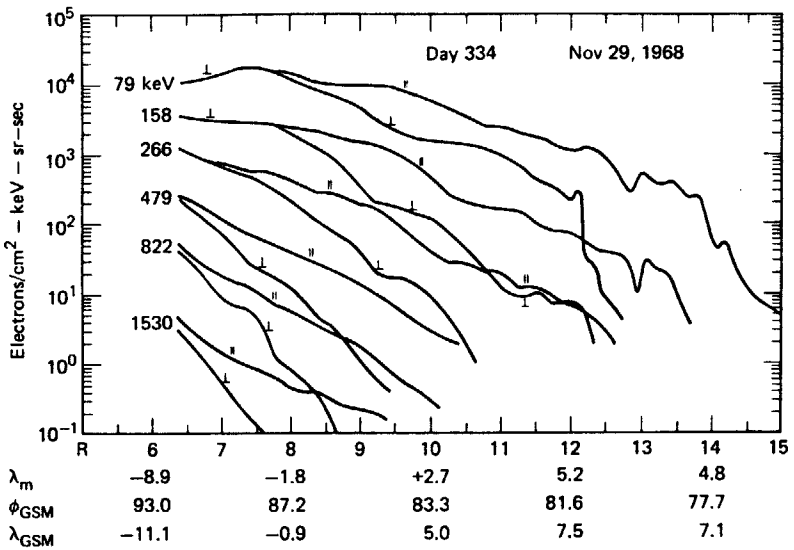
Day 334
Nov 29, 1968
79 keV
158
266
479
822
1530
Electrons/cm² – keV – sr–sec
R
λm
φGSM
λGSM
6
7
8
9
10
11
12
13
14
15
–8.9
–1.8
+2.7
5.2
4.8
93.0
87.2
83.3
81.6
77.7
–11.1
–0.9
5.0
7.5
7.1

West - Fig. 12

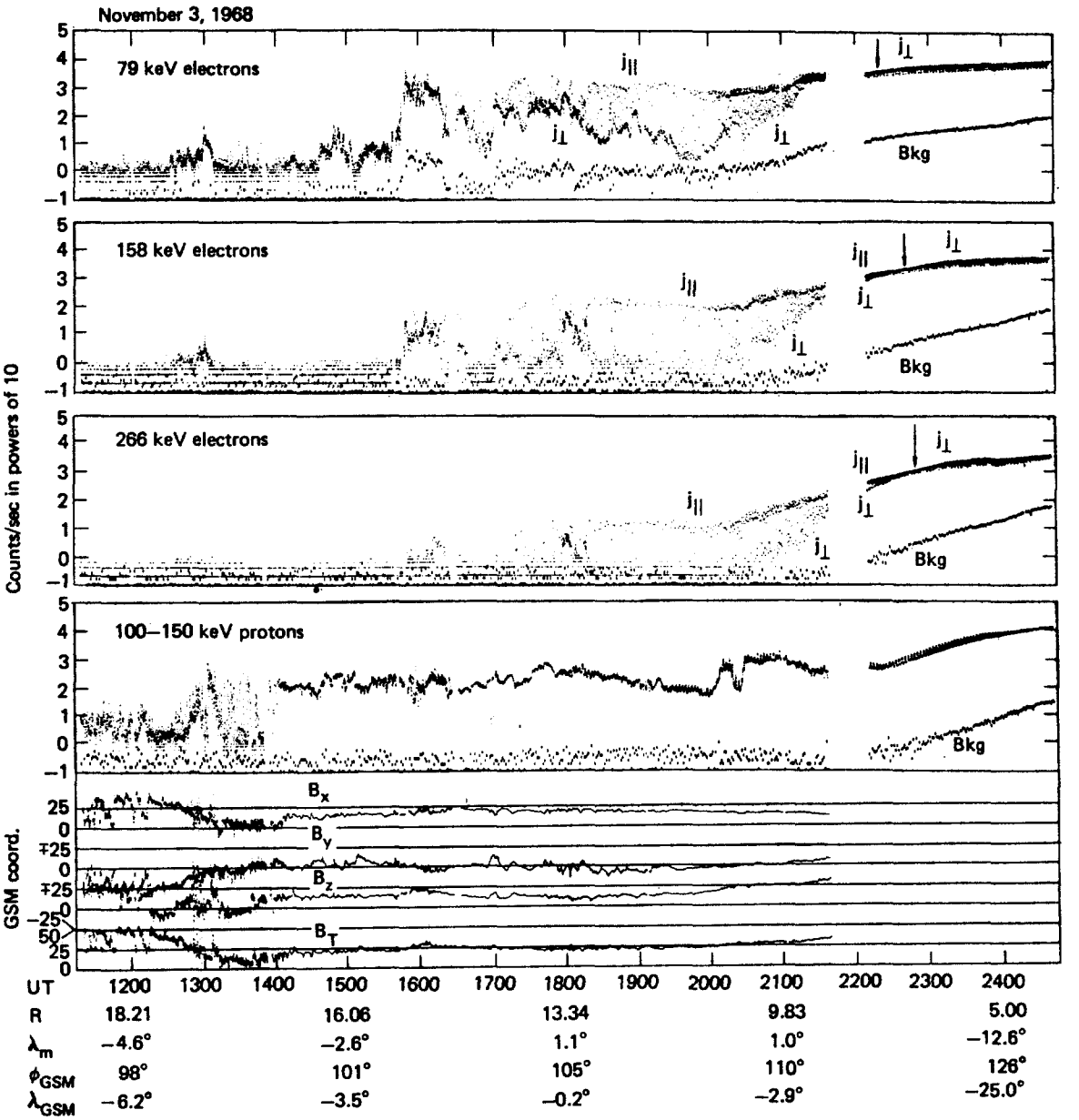
November 3, 1968
79 keV electrons
158 keV electrons
266 keV electrons
100–150 keV protons
Counts/sec in powers of 10
GSM coord.
Bkg
UT
1200 1300 1400 1500 1600 1700 1800 1900 2000 2100 2200 2300 2400
R 18.21 16.06 13.34 9.83 5.00
λm −4.6° −2.6° 1.1° 1.0° −12.6°
φGSM 98° 101° 105° 110° 126°
λGSM −6.2° −3.5° −0.2° −2.9° −25.0°

West - Fig. 13

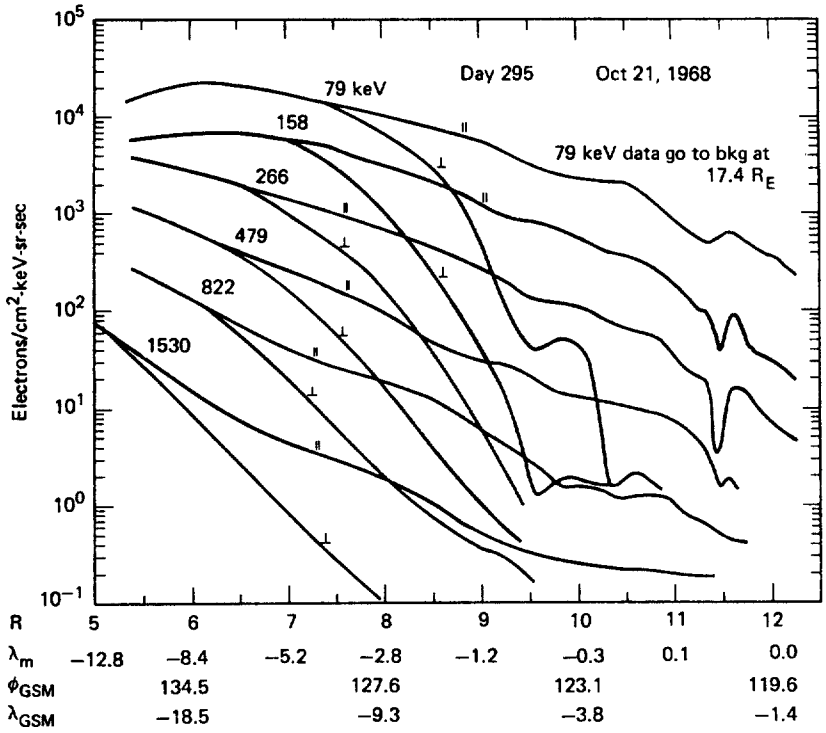
Day 295 Oct 21, 1968
79 keV
158
266
479
822
1530
79 keV data go to bkg at 17.4 R_E
Electrons/cm^2-keV-sr-sec
10^5
10^4
10^3
10^2
10^1
10^0
10^{-1}
R 5 6 7 8 9 10 11 12
λ_m −12.8 −8.4 −5.2 −2.8 −1.2 −0.3 0.1 0.0
ϕ_{GSM} 134.5 127.6 123.1 119.6
λ_{GSM} −18.5 −9.3 −3.8 −1.4

West - Fig. 14

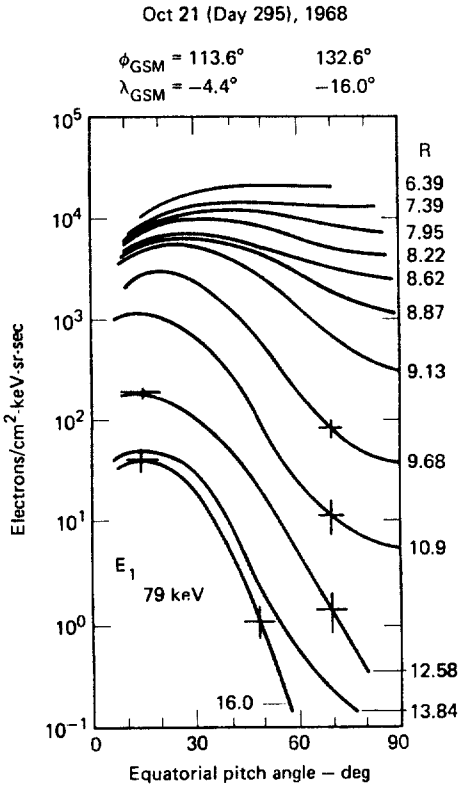
Oct 21 (Day 295), 1968
ϕ_{GSM} = 113.6° 132.6°
λ_{GSM} = −4.4° −16.0°
R
6.39
7.39
7.95
8.22
8.62
8.87
9.13
9.68
10.9
12.58
13.84
16.0
E_1
79 keV
Electrons/cm^2-keV-sr-sec
10^5
10^4
10^3
10^2
10^1
10^0
10^{-1}
0
30
60
90
Equatorial pitch angle — deg

West - Fig. 15

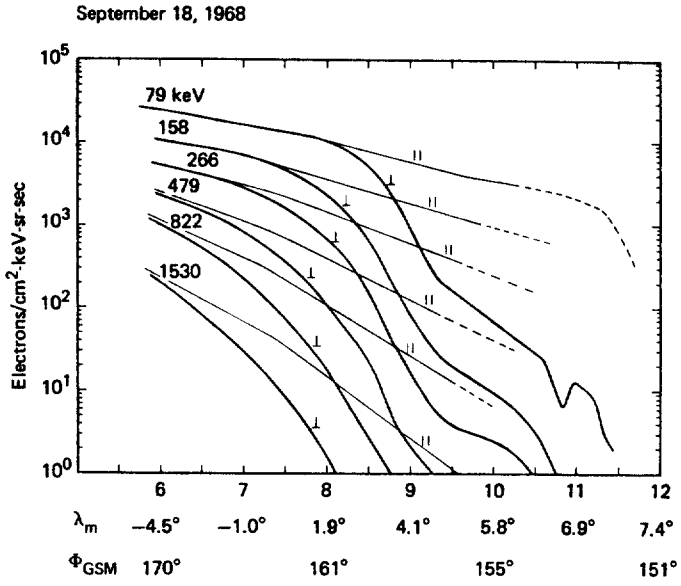
September 18, 1968
Electrons/cm²-keV-sr-sec
79 keV
158
266
479
822
1530
λm −4.5° −1.0° 1.9° 4.1° 5.8° 6.9° 7.4°
ΦGSM 170° 161° 155° 151°

West - Fig. 16

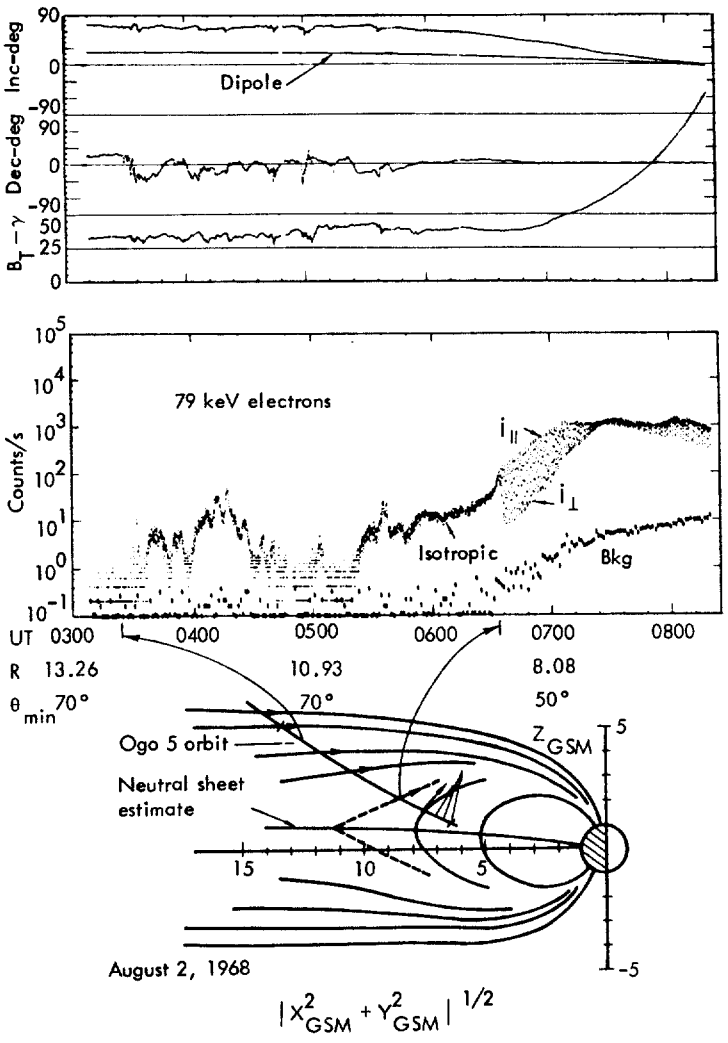
Inc-deg
Dec-deg
$B_T - \gamma$
90
0
-90
90
0
-90
50
25
0
Dipole
10^5
10^4
10^3
10^2
10^1
10^0
10^{-1}
Counts/s
79 keV electrons
$i_{\parallel}$
$i_{\perp}$
Isotropic
Bkg
UT 0300
0400
0500
0600
0700
0800
R 13.26
10.93
8.08
θ_{min} 70°
70°
50°
Ogo 5 orbit
Neutral sheet estimate
Z_{GSM}
5
-5
15
10
5
August 2, 1968
$|X^2_{GSM} + Y^2_{GSM}|^{1/2}$

West - Fig. 17

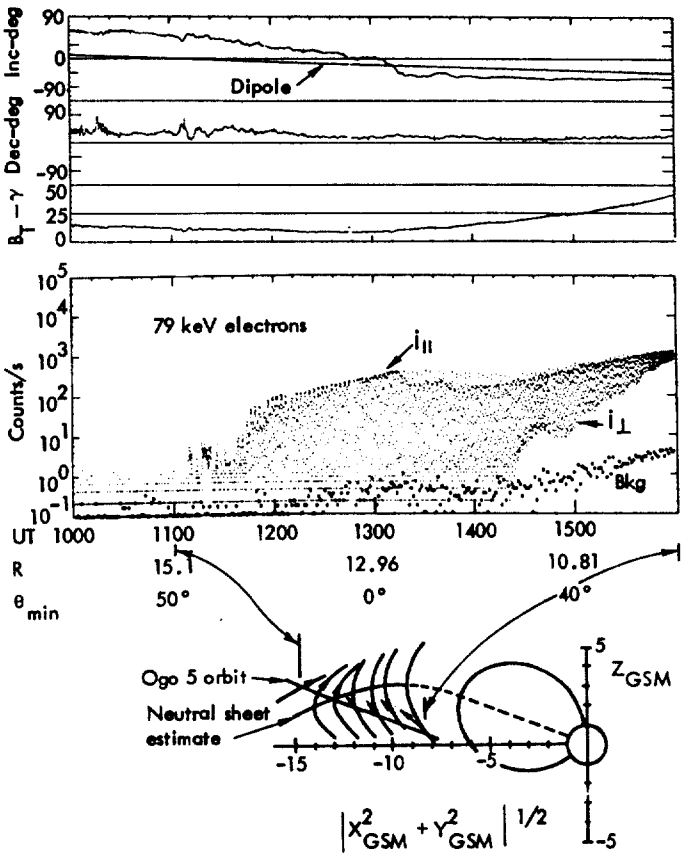
Inc-deg
Dec-deg
B_T – γ
90
0
-90
90
-90
50
25
0
Dipole
79 keV electrons
$i_{\parallel}$
$i_{\perp}$
Bkg
Counts/s
10^5
10^4
10^3
10^2
10^1
10^0
10^{-1}
UT 1000 1100 1200 1300 1400 1500
R 15.1 12.96 10.81
θ_{min} 50° 0° 40°
Ogo 5 orbit
Neutral sheet estimate
Z_{GSM}
5
-5
-15
-10
-5
$|X^2_{GSM} + Y^2_{GSM}|^{1/2}$
August 25, 1968

West - Fig. 18

August 9–10, 1968

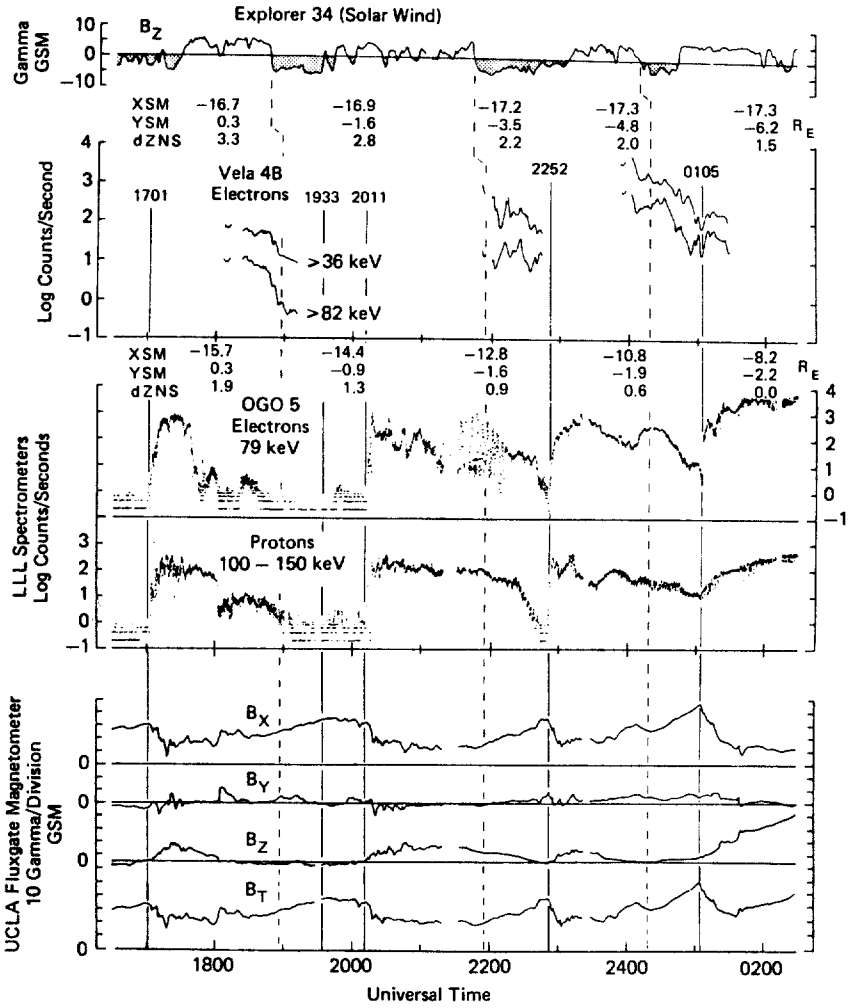

West - Fig. 19

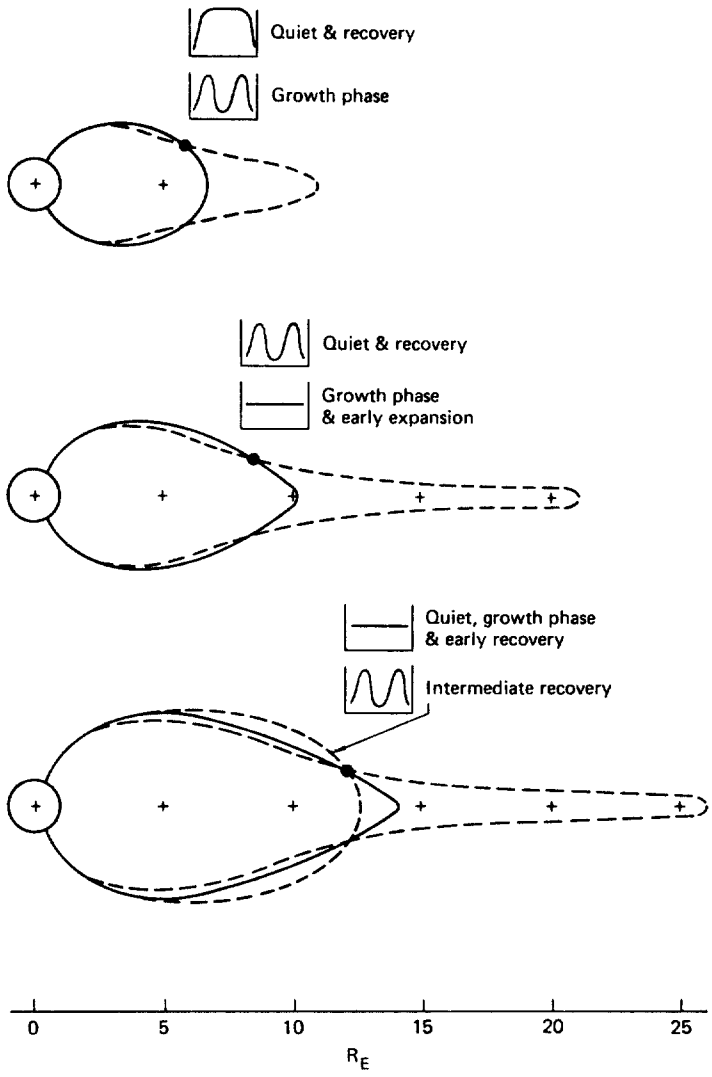
Quiet & recovery
Growth phase
Quiet & recovery
Growth phase
& early expansion
Quiet, growth phase
& early recovery
Intermediate recovery
0
5
10
15
20
25
R_E

West - Fig. 20

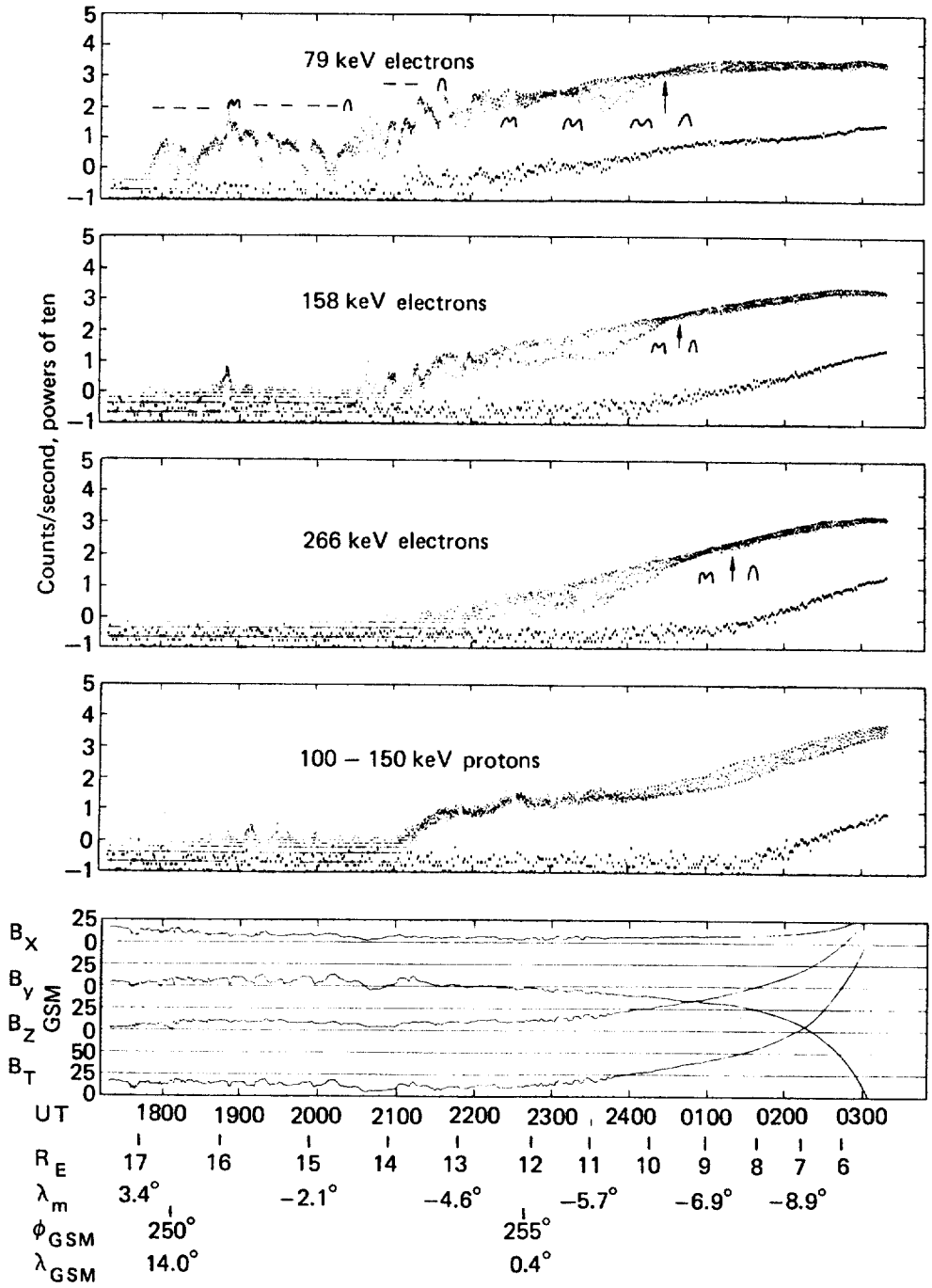
79 keV electrons
158 keV electrons
266 keV electrons
100 – 150 keV protons
Counts/second, powers of ten
B_X
B_y
B_Z
B_T
GSM
UT
1800
1900
2000
2100
2200
2300
2400
0100
0200
0300
R_E
17
16
15
14
13
12
11
10
9
8
7
6
λ_m
3.4°
−2.1°
−4.6°
−5.7°
−6.9°
−8.9°
ϕ_{GSM}
250°
255°
λ_{GSM}
14.0°
0.4°

West - Fig. 21

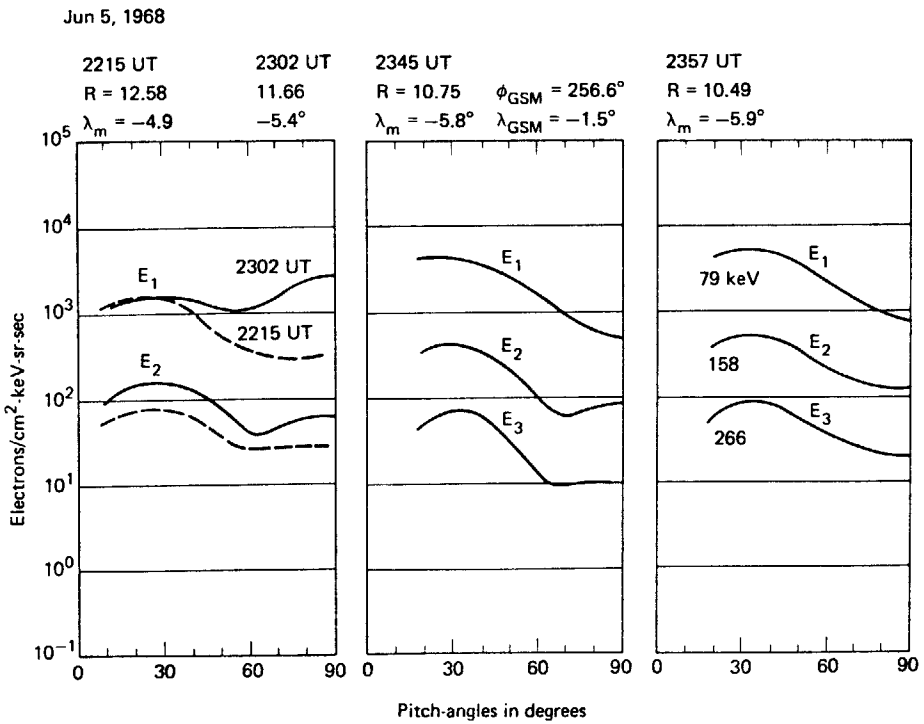
Jun 5, 1968
2215 UT
R = 12.58
λ_m = −4.9
2302 UT
11.66
−5.4°
2345 UT
R = 10.75
λ_m = −5.8°
ϕ_{GSM} = 256.6°
λ_{GSM} = −1.5°
2357 UT
R = 10.49
λ_m = −5.9°
Electrons/cm^2-keV-sr-sec
10^5
10^4
10^3
10^2
10^1
10^0
10^{-1}
E_1
2302 UT
2215 UT
E_2
E_1
E_2
E_3
E_1
79 keV
E_2
158
E_3
266
0
30
60
90
Pitch-angles in degrees

West - Fig. 22

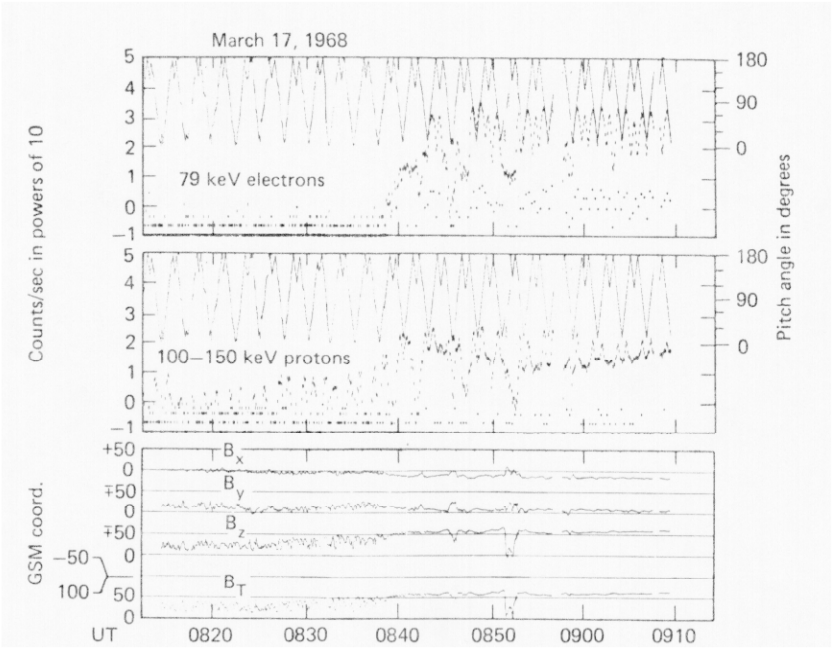

R	11.71	10.64
λ_m	8.5°	9.4°
ϕ_{GSM}	330°	332°
λ_{GSM}	15.5°	14.5°

West - Fig. 23

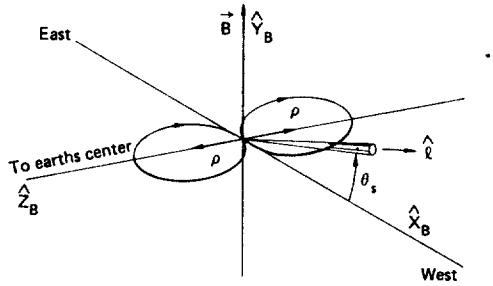
East
$\vec{B}$
$\hat{Y}_B$
ρ
ρ
$\hat{\ell}$
To earths center
$\hat{Z}_B$
θ_s
$\hat{X}_B$
West

West - Fig. 24

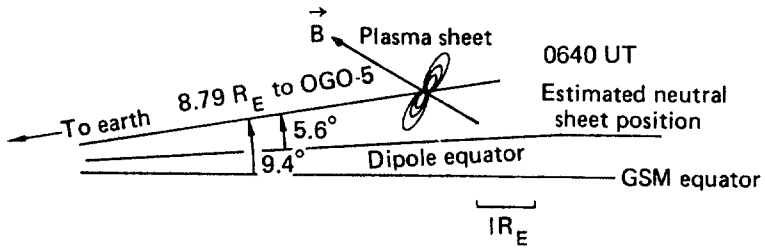
B
Plasma sheet
0640 UT
8.79 R_E to OGO-5
To earth
5.6°
Estimated neutral sheet position
9.4°
Dipole equator
GSM equator
1 R_E

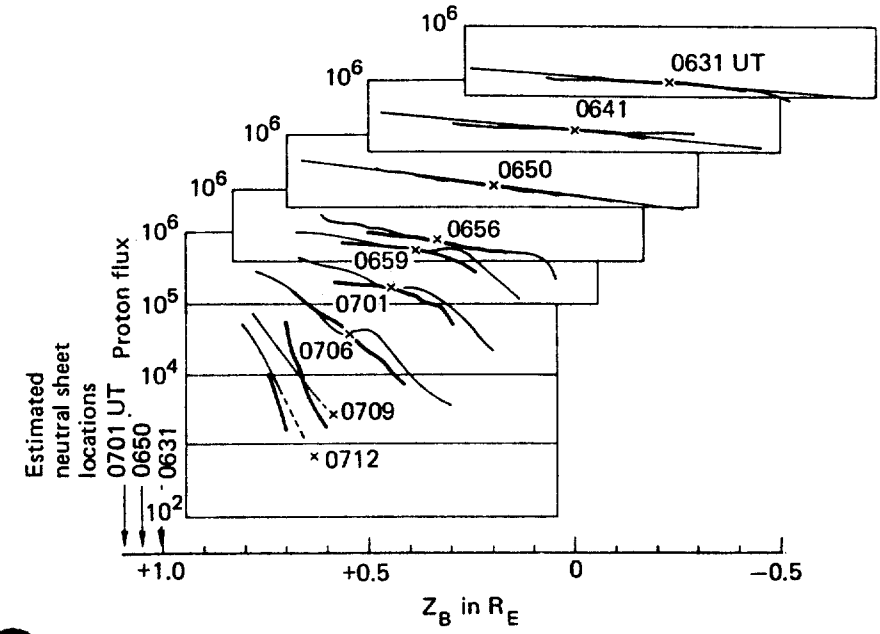
10^6
10^6
10^6
10^6
10^6
10^5
10^4
10^2
Proton flux
Estimated neutral sheet locations
0701 UT
0650
0631
0631 UT
0641
0650
0656
0659
0701
0706
0709
0712
+1.0
+0.5
0
−0.5
Z_B in R_E

West - Fig. 25